

Long Sequence Hopfield Memory

Hamza Tahir Chaudhry,^{1,2,*} Jacob A. Zavatone-Veth,^{3,2,†} Dmitry Krotov,^{4,‡} and Cengiz Pehlevan^{1,2,5,§}

¹*John A. Paulson School of Engineering and Applied Sciences,
Harvard University, Cambridge, Massachusetts 02138, USA*

²*Center for Brain Science, Harvard University, Cambridge, Massachusetts 02138, USA*

³*Department of Physics, Harvard University, Cambridge, Massachusetts 02138, USA*

⁴*MIT-IBM Watson AI Lab, IBM Research, Cambridge, Massachusetts 02142, USA*

⁵*Kempner Institute for the Study of Natural and Artificial Intelligence,
Harvard University, Cambridge, Massachusetts 02138, USA*

(Dated: June 7, 2023)

Sequence memory is an essential attribute of natural and artificial intelligence that enables agents to encode, store, and retrieve complex sequences of stimuli and actions. Computational models of sequence memory have been proposed where recurrent Hopfield-like neural networks are trained with temporally asymmetric Hebbian rules. However, these networks suffer from limited sequence capacity (maximal length of the stored sequence) due to interference between the memories. Inspired by recent work on Dense Associative Memories, we expand the sequence capacity of these models by introducing a nonlinear interaction term, enhancing separation between the patterns. We derive novel scaling laws for sequence capacity with respect to network size, significantly outperforming existing scaling laws for models based on traditional Hopfield networks, and verify these theoretical results with numerical simulation. Moreover, we introduce a generalized pseudoinverse rule to recall sequences of highly correlated patterns. Finally, we extend this model to store sequences with variable timing between states' transitions and describe a biologically-plausible implementation, with connections to motor neuroscience.

I. INTRODUCTION

Memory is an essential ability of intelligent agents that allows them to encode, store, and retrieve information and behaviors they have learned throughout their lives. In particular, the ability to recall sequences of memories is necessary for a large number of cognitive tasks with temporal or causal structure, including navigation, reasoning, and motor control [1–9].

Computational models have been proposed for how neural networks can encode sequence memory, ranging across a wide range of biological plausibility [1–3, 10–21]. Many of these are based on the concept of associative memory, also known as content-addressable memory, which refers to the ability of a system to recall a set of objects or ideas when prompted by a distortion or subset of them. Modeling associative memory has been an extremely active area of research in computational neuroscience and deep learning for many years, with the Hopfield network becoming the canonical model [22–24].

Unfortunately, a major limitation of the traditional Hopfield Network and related associative memory models is its capacity: the number of memories it can store and reliably retrieve scales linearly with the number of neurons in the network. This limitation is due to interference between different memories during recall, also known as crosstalk, which decreases the signal-to-noise ratio. Large amount of crosstalk results in the recall of incorrect local minima, which are undesired attractor states of the network commonly referred to as spin glass states [25–28].

Recent modifications of the Hopfield Network, known as Dense Associative Memories or Modern Hopfield Networks (MHNs), overcome this limitation by introducing a strong nonlinearity when computing the overlap between the state of the network and memory patterns stored in the network [29, 30]. This leads to a greater separation between partially overlapping memories, thereby reducing the crosstalk, increasing the signal-to-noise ratio, and increasing the probability of successful recall [31].

Most models based on the Hopfield Network are autoassociative, meaning they are designed for the robust storage and recall of individual memories. Thus, they are incapable of storing sequences of memories. In order to adapt these models to store sequences, one must utilize asymmetric weights in order to drive the network from one activity pattern to the next. Many such models use temporally asymmetric Hebbian learning rules to strengthen synaptic connections

* hchaudhry@g.harvard.edu

† jzavatoneveth@g.harvard.edu

‡ krotov@ibm.com

§ cpehlevan@seas.harvard.edu

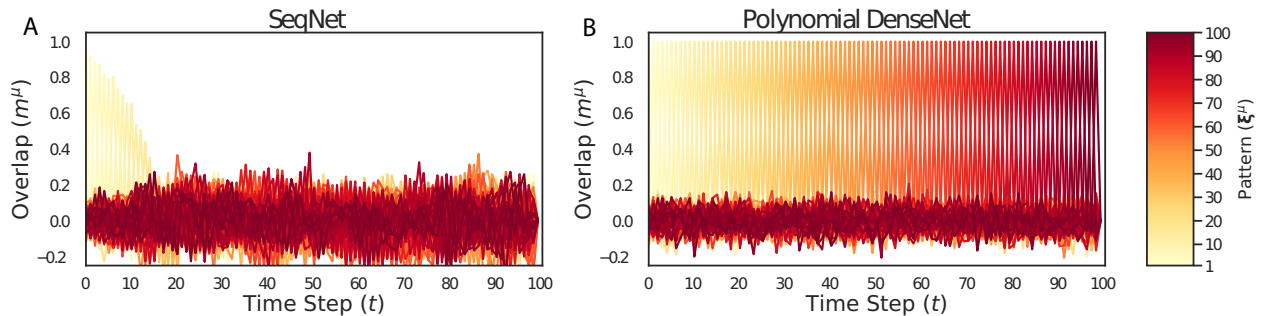


FIG. 1. SeqNet and Polynomial DenseNet ($d = 2$) are simulated with $N = 300$ neurons and $P = 100$ patterns. One hundred curves are plotted as a function of time, each representing the overlap of the network state at time t with one of the patterns, $m^\mu = (1/N) \sum_{i=1}^N \xi_i^\mu S_i$. The curves are ordered using the color code described on the right (patterns in the beginning and end of the sequence are shaded in yellow and red respectively). (A) SeqNet quickly loses the correct sequence, indicated by the lack of alignment of the network state with the correct pattern in the sequence ($m^\mu \ll 1$). (B) The Polynomial DenseNet faithfully recalls the entire sequence and maintains alignment with one of the patterns at any moment in time, $m^\mu \approx 1$.

between neural activity at one time state and the next time state, thereby learning temporal association between patterns in a sequence [1, 3, 10, 11, 16, 17].

In this paper, we extend Dense Associative Memories to the setting of asymmetric weights in order to store and recall long sequences of memories. A related model was recently studied by Karuvally *et al.* [32] where they leveraged an adiabatic approach on the energy landscape of Hopfield Networks. In contrast, we work directly with the update rule for the state of the network, allowing us to provide an analytical derivation for the sequence capacity of our proposed network. We find a close match between theoretical calculation and numerical simulation, and further establish the ability of this model to store and recall sequences of correlated patterns. Additionally, we extend this model to store sequences with repeated patterns through temporal association across longer timescales. Also, we examine the dynamics of a model containing both symmetric and asymmetric terms. Finally, we describe applications of our network as a model of biological motor control.

II. DENSENETS FOR SEQUENCE STORAGE

Traditional Hopfield Networks and Modern Hopfield Networks, as described in Appendix B, are capable of storing individual memories. What about storing sequences?

Assume that we want to store a sequence of P patterns, $\{\xi^1, \dots, \xi^P\}$, where $\xi_j^\mu \in \{\pm 1\}$ is the j^{th} neuron of the μ^{th} pattern and the network will transition from pattern ξ^μ to $\xi^{\mu+1}$. Let N be the number of neurons in the network and $\mathbf{S}(t) \in \{-1, +1\}^N$ be the state of the network at time t . We want to design a network with dynamics such that when the network is initialized in pattern ξ^1 , it will traverse the entire sequence¹. We define a network, SeqNet, which follows a discrete-time synchronous update rule²:

$$T_{SN}(\mathbf{S})_i := \text{sgn} \left[\sum_{j \neq i} J_{ij} S_j \right] = \text{sgn} \left[\sum_{\mu=1}^P \xi_i^{\mu+1} m_i^\mu \right], \quad m_i^\mu := \frac{1}{(N-1)} \sum_{j \neq i} \xi_j^\mu S_j, \quad (1)$$

where $\mathbf{S}(t+1) = T_{SN}(\mathbf{S})$ and $J_{ij} = \frac{1}{N} \sum_{\mu=1}^P \xi_i^{\mu+1} \xi_j^\mu$ is an asymmetric matrix connecting pattern ξ^μ to $\xi^{\mu+1}$. Note that we are excluding self-interaction terms $i = j$. We rewrite the dynamics in terms of m_i^μ , the overlap of the network state \mathbf{S} with pattern ξ^μ . When the network is aligned most closely with pattern ξ^μ , the overlap m_i^μ is the largest contribution in the sum and pushes the network to pattern $\xi^{\mu+1}$. When multiple patterns have similar overlaps, meaning they are correlated, then there will be low signal-to-noise ratio. This correlation between patterns limits the capacity of the network, limiting the SeqNet's capacity to scale linearly relative to network size.

¹ For convenience, we impose periodic boundary conditions and define $\xi_i^{P+1} \equiv \xi_i^1$. Boundary terms have a sub-leading contribution to the crosstalk, and so a model without periodic boundary conditions will have the same scaling of capacity.

² One can also consider an asynchronous update rule in which a single neuron is updated at each timestep [23, 25].

To overcome the capacity limitations of the SeqNet, we use inspiration from Dense Associative Memories to define the DenseNet update rule:

$$T_{DN}(\mathbf{S})_i := \text{sgn} \left[\sum_{\mu=1}^P \xi_i^{\mu+1} f(m_i^\mu) \right] \quad (2)$$

where f is a nonlinear monotonically increasing interaction function. Similar to MHNs, f reduces the crosstalk between patterns and, as we will analyze in detail, leads to improved capacity. Figure 1 demonstrates this improvement for $f(x) = x^2$.

A. Sequence capacity

To derive analytical results for the capacity, we must choose a distribution to generate the patterns. As is standard in studies of the classic HN and MHNs [25–30, 33–36], we choose this to be the Rademacher distribution, where $\xi_j^\mu \in \{-1, +1\}$ with equal probability for all neurons j in all patterns μ , and calculate the capacity for different update rules. We consider both the robustness of a single transition, and the robustness of propagation through the full sequence. For a fixed network size $N \in \{2, 3, \dots\}$ and an error tolerance $c \in [0, 1)$, we define the single-transition and sequence capacities by

$$P_T(N, c) = \max \{P \in \{2, \dots, 2^N\} : \mathbb{P}[\mathbf{T}_{DN}(\boldsymbol{\xi}^1) = \boldsymbol{\xi}^2] \geq 1 - c\} \quad (3)$$

and

$$P_S(N, c) = \max \{P \in \{2, \dots, 2^N\} : \mathbb{P}[\cap_{\mu=1}^P \{\mathbf{T}_{DN}(\boldsymbol{\xi}^\mu) = \boldsymbol{\xi}^{\mu+1}\}] \geq 1 - c\}, \quad (4)$$

respectively, where the probability is taken over the random patterns. Note that the full sequence capacity is defined by demanding that all transitions are correct. For perfect recall, we want to take the threshold $c \downarrow 0$. In the thermodynamic limit in which $N, P \rightarrow \infty$, we expect for there to exist a sharp transition in the recall probabilities as a function of P , with almost-surely perfect recall below the threshold value and vanishing probability of recall above [25–28, 30, 33–36]. Thus, we expect the capacity to become insensitive to the value of c in the thermodynamic limit; this is known rigorously for the classic Hopfield network from the work of Bovier [34].

As we detail in Appendix C, all of our theoretical results are obtained under two approximations. We will validate the accuracy of the resulting capacity predictions through comparison with numerical experiments. First, following Petritis [33]’s analysis of the classic Hopfield network, we use union bounds to control the single-transition and full-sequence capacities in terms of the single-bitflip error probability $\mathbb{P}[T_{DN}(\boldsymbol{\xi}^1)_1 \neq \xi_1^2]$. Using the fact that the patterns are i.i.d., this gives $\mathbb{P}[\mathbf{T}_{DN}(\boldsymbol{\xi}^\mu) = \boldsymbol{\xi}^{\mu+1}] \geq 1 - N\mathbb{P}[T_{DN}(\boldsymbol{\xi}^1)_1 \neq \xi_1^2]$ and $\mathbb{P}[\cap_{\mu=1}^P \{\mathbf{T}_{DN}(\boldsymbol{\xi}^\mu) = \boldsymbol{\xi}^{\mu+1}\}] \geq 1 - NP\mathbb{P}[T_{DN}(\boldsymbol{\xi}^1)_1 \neq \xi_1^2]$, respectively, resulting in the lower bounds

$$P_T(N, c) \geq \max \{P \in \{2, \dots, 2^N\} : N\mathbb{P}[T_{DN}(\boldsymbol{\xi}^1)_1 \neq \xi_1^2] \leq c\}, \quad (5)$$

$$P_S(N, c) \geq \max \{P \in \{2, \dots, 2^N\} : NP\mathbb{P}[T_{DN}(\boldsymbol{\xi}^1)_1 \neq \xi_1^2] \leq c\}. \quad (6)$$

From studies of the classic Hopfield network, we expect for these bounds to be tight in the thermodynamic limit ($N \rightarrow \infty$), but we will not attempt to prove that this is so [33, 34]. Second, our theoretical results are obtained under the approximation of $\mathbb{P}[T_{HN}(\boldsymbol{\xi}^1)_1 \neq \xi_1^2]$ in the regime $N, P \gg 1$ by a Gaussian tail probability. Concretely, we write the single-bitflip probability as

$$\mathbb{P}[T_{DN}(\boldsymbol{\xi}^1)_1 \neq \xi_1^2] = \mathbb{P}[C < -f(1)] \quad (7)$$

in terms of the crosstalk

$$C = \sum_{\mu=2}^P \xi_1^2 \xi_1^{\mu+1} f\left(\frac{1}{N-1} \sum_{j=2}^N \xi_j^\mu \xi_j^1\right), \quad (8)$$

which represents interference between patterns that can lead to a bitflip. Then, as the crosstalk is the sum of $P - 1$ i.i.d. random variables, we approximate its distribution as Gaussian. We then extract the capacity by determining how P should scale with N such that the error probability tends to zero as $N \rightarrow \infty$, corresponding to taking $c \rightarrow 0$ with increasing N . Within the Gaussian approximation, we can also determine the capacity at fixed c by using the asymptotics of the inverse Gaussian tail distribution function to determine how P should scale with N such that the

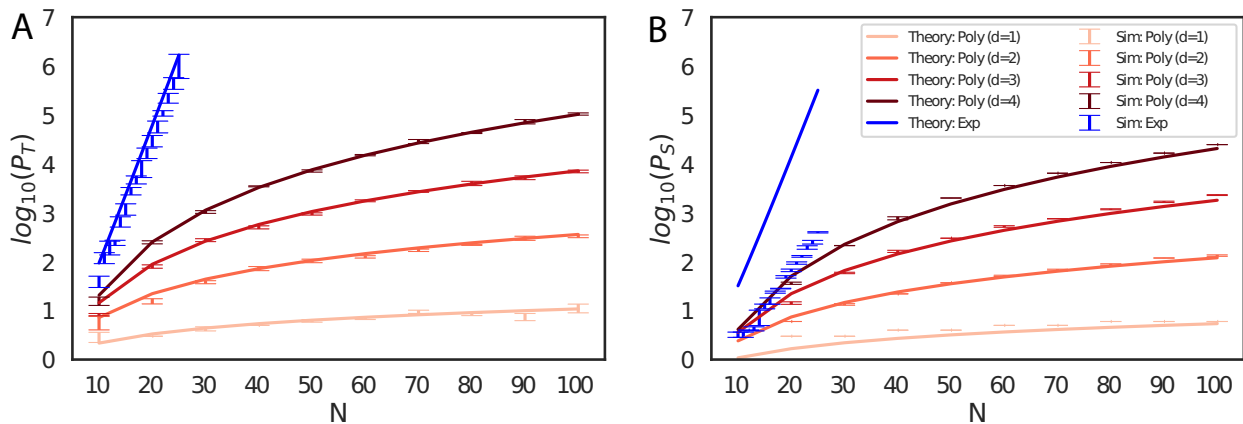


FIG. 2. The transition and sequence capacities are tested for DenseNets with polynomial and exponential nonlinearities. 100 Sequences of P Rademacher-distributed patterns are generated, the update rule is applied, and the amount of errors is calculated. If there are any errors, then the sequence is considered unstable and a smaller sequence is tested. This is repeated until 100 independent sequences of length P are recalled without error. Error bars are calculated by repeating this entire process for 20 different initializations. As network size increases, the variance of the crosstalk decreases and the theoretical approximations become more accurate, resulting in a tight match between theory (solid lines) and simulation (points with error bars). Transition capacity $\log_{10}(P_T)$ is plotted on the left. Sequence capacity $\log_{10}(P_S)$ is plotted on the right. The theory curves are given by Equations 9 and 10. There is significant deviation between theory and simulation for the sequence capacity of the Exponential DenseNet. We show that this is due to finite-size effects in Section II C. See Appendix F for details of our numerical methods.

error probability is asymptotically bounded by c as $N \rightarrow \infty$. This predicts that the effect of non-negligible c should vanish as $N \rightarrow \infty$.

For P large but finite, this Gaussian approximation amounts to retaining only the leading term in the asymptotic Edgeworth expansion of the tail distribution function [37–40]. We will not endeavour to rigorously control the error of this approximation in the regime of interest in which N is also large. To convert our heuristic results into fully rigorous asymptotics, one would want to construct an Edgeworth-type series expansion for the tail probability $\mathbb{P}[C < -f(1)]$ that is valid in the joint limit with rigorously-controlled asymptotic error, accounting for the fact that the crosstalk is a sum of discrete random variables [37–40]. As a simple probe of Gaussianity, we will consider the excess kurtosis of the crosstalk distribution, which determines the leading correction to the Gaussian approximation in the Edgeworth expansion, and describes whether its tails are heavier or narrower than Gaussian [37–40].

B. Polynomial DenseNet

Consider the DenseNet with polynomial interaction function, $f(x) = x^d$, which we will call the Polynomial DenseNet. In Appendix C 1, we argue that the leading asymptotics of the transition and sequence capacities for perfect recall are given by

$$P_T \sim \frac{N^d}{2(2d-1)!! \log(N)}, \quad P_S \sim \frac{N^d}{2(d+1)(2d-1)!! \log(N)}. \quad (9)$$

Note that this polynomial scaling of the single-transition capacity with network size coincides with the capacity scaling of the symmetric Modern Hopfield Network [29]. Indeed, as we have excluded self-interaction terms in the update rule, the single-bitflip probabilities for these two models coincide exactly (Appendix C 1). We compare our results for the single-transition and sequence capacities to numerical simulation in Figure 2. The simulation matches theoretical prediction for large network size N . For smaller N , there are finite-size effects that result in deviation from theoretical prediction. The crosstalk has non-negligible kurtosis in finite size networks which leads to deviation from the Gaussian approximation.

Furthermore, we point out that for fixed N , the network capacity does not monotonically increase in the degree d . Since the factorial function grows faster than the exponential function, every finite network of size N has a polynomial degree d_{max} after which the capacity will actually decrease. This is also true for the standard MHN. We demonstrate this numerically in Figure 3, again noting mild deviations between theory and simulation due to finite-size effects.

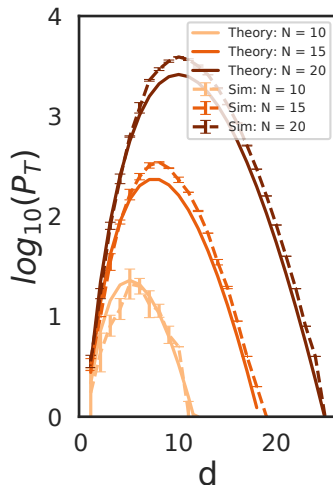


FIG. 3. Transition Capacity of Polynomial DenseNets as a function of polynomial degree. For any finite network size N , there is a degree d_T that bounds the maximum transition capacity. The same would be true for the sequence capacity.

C. Exponential DenseNet

We have shown the DenseNet’s capacity can scale polynomially with network size. Can it scale exponentially? Consider the DenseNet with exponential interaction function, $f(x) = e^{(N-1)(x-1)}$, which we call the Exponential DenseNet. This function reduces crosstalk dramatically: $f(m^\mu(\mathbf{S})) = 1$ when $m^\mu(\mathbf{S}) = 1$ and is otherwise sent to 0 exponentially fast. In Appendix C 2, we show that under the abovementioned approximations one has the leading asymptotics

$$P_T \sim \frac{\beta^{N-1}}{2 \log N} \quad \text{and} \quad P_S \sim \frac{\beta^{N-1}}{2 \log(\beta)N}, \quad \text{where} \quad \beta = \frac{\exp(2)}{\cosh(2)} \simeq 1.964 \dots \quad (10)$$

In Figure 2, numerical simulations confirm this model scales significantly better than the Polynomial DenseNet and enables one to store exponentially long sequences relative to network size. While the relative gap between single-transition and full-sequence capacities remains bounded for the Polynomial DenseNet, where $P_T/P_S \sim d + 1$, the gap for the Exponential DenseNet diverges with network size.

However, we can see in Figure 2 that the empirically measured capacity—particularly the sequence capacity—of the Exponential DenseNet deviates substantially from the predictions of our approximate Gaussian theory. Due to computational constraints, our numerical simulations are limited to small network sizes (Appendix F). Computing the excess kurtosis of the crosstalk distribution with a number of patterns comparable to the capacity predicted by the Gaussian theory reveals that, for the range of system sizes we can simulate, the distribution should deviate strongly from a Gaussian. In particular, if take $P \sim \beta^{N-1}/(\alpha N)$ for some constant factor α , then the excess kurtosis increases with network size up to around $N \approx 56$ (Appendix C 2). Increasing the size of an Exponential DenseNet therefore has competing effects: for a fixed sequence length P , increasing network size N decreases the crosstalk variance, which should reduce the bitflip probability, but also increases the excess kurtosis, which reflects a fattening of the crosstalk distribution tails that should increase the bitflip probability. This is illustrated in Figure 4.

The competition between increasing P and N for the Exponential DenseNet is easy to understand intuitively. For a fixed N , increasing P means that the crosstalk is equal in distribution to the sum of an increasingly large number of i.i.d. random variables, and thus by the central limit theorem should become increasingly Gaussian. Conversely, for a fixed P , increasing N means that each of the $P - 1$ contributions to the crosstalk is equal in distribution to the product of an increasing number of i.i.d. random variables—as $f(\frac{1}{N-1} \sum_{j=2}^N \xi_j^\mu \xi_j^1) = \prod_{j=2}^N \exp(\xi_j^\mu \xi_j^1)$ —and thus by the multiplicative central limit theorem each term should tend to a lognormal distribution. In this regime, then, the crosstalk is roughly a mixture of lognormals, which is decidedly non-Gaussian. In contrast, for a Polynomial DenseNet, memorization is easy in the limit where N tends to infinity for fixed P , as the crosstalk should tend almost surely to zero as each term $f(\frac{1}{N-1} \sum_{j=2}^N \xi_j^\mu \xi_j^1) \rightarrow 0$ almost surely.

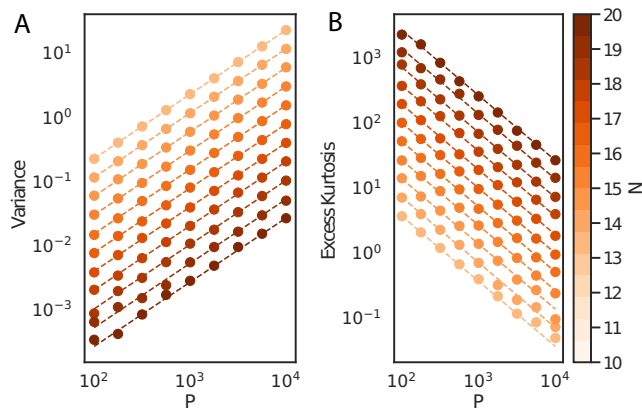


FIG. 4. Crosstalk statistics for the Exponential DenseNet as a function of P and N : (A) Variance plotted (B) Excess Kurtosis. The dots are simulation and lines are theory. Variance is proportional to P and inversely proportional to N , while the opposite is true for excess kurtosis.

D. Recalling Sequences of Correlated Patterns

The full-sequence capacity scaling laws for these models were derived under the assumption of i.i.d Rademacher random patterns. While theoretically convenient, this is unrealistic for real-world data. We therefore test these networks in more realistic settings by storing correlated sequences of patterns, which will lead to greater crosstalk in each transition and a smaller single-transition and full-sequence capacities relative to network size [25, 36]. However, the nonlinear interaction functions should still assist in separating correlated patterns to enable successful sequence recall.

For demonstration, we store a sequence of 10000 binarized MNIST images using DenseNets and compared the recall of these images using different nonlinearities. The entire sequence is composed of 1000 subsequences of unique hand-written images of digits ranging from 0 to 9. Since there are 1000 examples of each digit across the entire sequence, significant correlation between patterns results in large amounts of crosstalk. The results of the DenseNets are shown in Figure 5, where increasing the nonlinearity of the Polynomial DenseNets improves recall but not entirely, except for the exponential network which achieves perfect recall. Note that SeqNet and DenseNet ($d = 5$) return

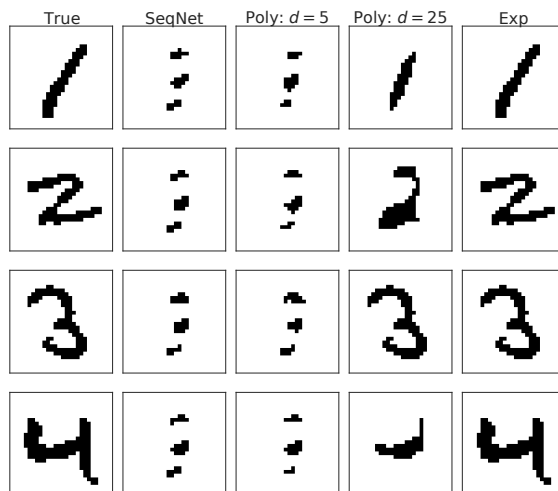


FIG. 5. Recall of a sequence of 10000 binarized MNIST images using DenseNets of size $N = 28 \cdot 28 = 784$. The columns depict different nonlinearities. The rows depict network recall at time $T = 1, 102, 203, 304$. We chose these timesteps to see how the network reconstructs images further into the sequence, rather than just the first few. Conclusions hold for arbitrary choice of timesteps. See Appendix F for details of our numerical methods.

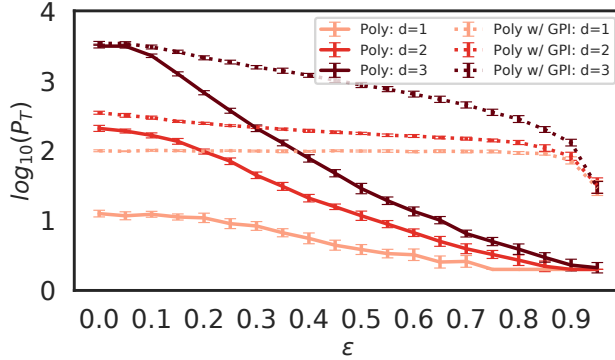


FIG. 6. Transition capacity of Polynomial DenseNets of size $N = 100$ relative to pattern correlation strength ϵ . Increasing ϵ monotonically decreases capacity. Networks with stronger nonlinearities maintain high capacity for large correlation strength. Implementing the generalized pseudoinverse rule decorrelates these patterns and maintains high sequence capacity for much larger correlation.

approximately the same state for all times, indicating these networks are stuck in metastable states. DenseNet ($d = 25$) has better recall, but observe that while it correctly recalls a digit 2, it is the wrong instance, likely due to the high correlation between images of the same digit. The Exponential DenseNet performs the best and perfectly recalls the true patterns.

E. Generalized pseudoinverse rule

Can we overcome the DenseNet’s limited ability to store correlated patterns? Drawing inspiration from the pseudoinverse learning rule introduced by Kanter and Sompolinsky [41] for the classic Hopfield network, we propose a generalized pseudoinverse (GPI) transition rule

$$T_{GPI}(\mathbf{S})_i := \text{sgn} \left[\sum_{\mu=1}^P \xi_i^{\mu+1} f \left(\sum_{\nu=1}^P (O^+)^{\mu\nu} m^\nu(\mathbf{S}) \right) \right], \quad O^{\mu\nu} = \frac{1}{N} \sum_{j=1}^N \xi_j^\mu \xi_j^\nu, \quad (11)$$

where the overlap matrix $O^{\mu\nu}$ is positive-semidefinite, so we can define its pseudoinverse \mathbf{O}^+ by inverting the non-zero eigenvalues. With $f(x) = x$, this reduces to the pseudoinverse rule.

If the patterns are linearly independent, such that \mathbf{O} is full-rank, we can see that this rule can perfectly recall the full sequence (Appendix D). This matches the classic pseudoinverse rule’s ability to perfectly store any set of linearly independent patterns; this is why we choose to sum over ν inside the separation function in (11). For i.i.d. Rademacher patterns, linear independence holds almost surely in the thermodynamic limit provided that $P < N$.

In Figure 6, we demonstrate the effect of correlation on the Polynomial DenseNet through studying the recall of biased patterns ξ_i^μ with $\mathbb{P}(\xi_i^\mu = \pm 1) = \frac{1}{2}(1 \pm \epsilon)$ for $\epsilon \in [0, 1]$.³ In Figure 6, we see that the Polynomial DenseNet has better recall at all levels of correlation ϵ as degree d increases, although we still expect there to be a large maximum degree as described before. However, at large correlation values, they all have low recall, suggesting the need for alternative methods to decorrelate these patterns. We show the generalized pseudoinverse update rule is more robust to large correlations than the standard Polynomial DenseNet. While this update rule also applies to the Exponential DenseNet, simulations fail due to numerical instability coming from small values in the pseudoinverse.

III. MIXEDNET FOR VARIABLE TIMING

Thus far, we have considered sequence recall in purely asymmetric networks. These networks transition to the next pattern in the sequence at every timestep, preventing the network from storing sequences with longer timing between

³ At $\epsilon = 1$, the patterns will be deterministic with $\xi_i^\mu = +1$.

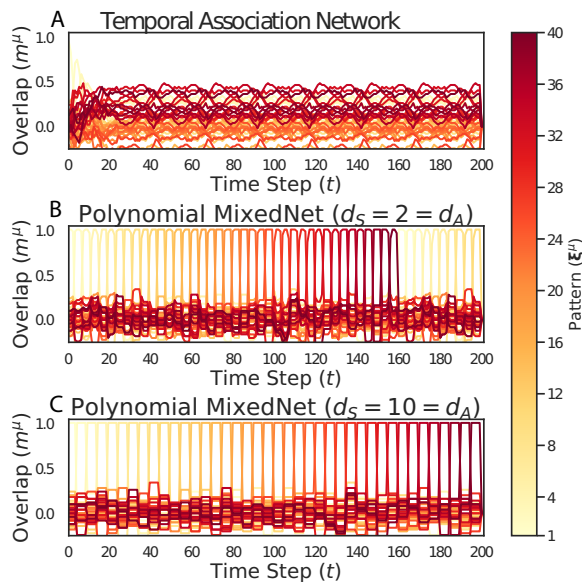


FIG. 7. We simulate MixedNets with $N = 100$, $\tau = 5$, and attempt to store $P = 40$ patterns. (A) The Temporal Association Network, corresponding to a linear MixedNet with $d_S = 1 = d_A$, fails to recover the sequence. (B) Increasing the nonlinearities to $d_S = 2 = d_A$ recovers the correct sequence order, but not the timing. (C) Increasing the nonlinearities to $d_S = 10 = d_A$ recovers the correct sequence order and timing.

elements. In this section, we aim to construct a model where the network stays in a pattern for τ steps. Our starting model will be an associative memory model for storing sequences known as the Temporal Association Network (TAN) [1, 10], defined as:

$$T_{TAN}(\mathbf{S})_i := \text{sgn} \left[\sum_{\mu=1}^P \left[\xi_i^\mu m_i^\mu + \lambda \xi_i^{\mu+1} \bar{m}_i^\mu \right] \right], \quad \bar{m}_i^\mu := \frac{1}{N-1} \sum_{j \neq i} \xi_j^\mu \bar{S}_j \quad (12)$$

where \bar{m}_i^μ represents the normalized overlap of each pattern ξ^μ with a weighted time-average of the network over the past τ timesteps, $\bar{S}_i(t) = \sum_{\rho=0}^{\tau-1} w(\rho) S_i(t - \rho)$. The weight function, $w(t)$, is generally taken to be a low-pass convolutional filter (e.g. Heaviside step function, exponential decay).

This network combines a symmetric and asymmetric term for robust recall of multiple sequences. The symmetric term containing $m_i^\mu(t)$, also referred to as a “fast” synapse, stabilizes the network in pattern ξ^μ for a desired amount of time. The asymmetric term containing $\bar{m}_i^\mu(t)$, also referred to as a “slow” synapse, drives the network transition to pattern $\xi^{\mu+1}$. The λ parameter controls the strength of the transition signal. If λ is too small, no transitions will occur since the symmetric term will overpower it. If λ is too large, transitions will occur too quickly for the network to stabilize in a desired pattern and the sequence will quickly destabilize.

For the Temporal Association Network, Sompolinsky and Kanter [10] used numerical simulations to estimate the capacity as approximately $P_{TAN} \sim 0.1N$, defining capacity as the ability to recall the sequence in correct order with high overlap (meaning that a small proportion of incorrect bits are allowed in each transition). Note that this model can fail in two ways: (i) it can fail to recall the correct sequence of patterns, or (ii) it can fail to stay in each state for the desired amount of time.

To address these issues, we consider the following dynamics:

$$T_{MN}(\mathbf{S})_i := \text{sgn} \left[\sum_{\mu=1}^P \left[\xi_i^\mu f_S(m_i^\mu) + \lambda \xi_i^{\mu+1} f_A(\bar{m}_i^\mu) \right] \right] \quad (13)$$

We call this model the MixedNet, and seek to analyze the relationship between the symmetric and asymmetric terms in driving network dynamics and their impact on sequence capacity. As before, the asymmetric term will try to push the network to the next state at every timestep, while the symmetric term tries to maintain it in its current state for τ timesteps. We will allow different nonlinearities for f_S and f_A , and analyze their effect on transition and sequence capacity.

We demonstrate the effectiveness of the Polynomial MixedNet, where for simplicity we set $f_S(x) = f_A(x) = x^d$, in Figure 7. While the Temporal Association Network fails completely, a polynomial nonlinearity of $d = 2$ enables recall

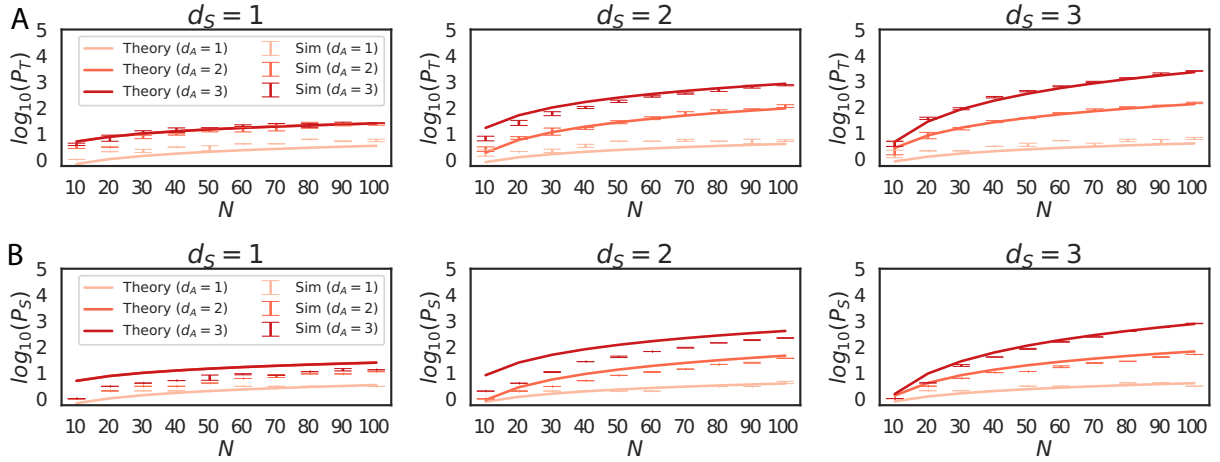


FIG. 8. (A) Transition capacity $\log_{10}(P_T)$ of the Polynomial MixedNet is plotted relative to network size. (B) Sequence capacity $\log_{10}(P_S)$ of the Polynomial MixedNet is plotted relative to network size. Each plot has a fixed symmetric nonlinearity $f_S(x) = x^{d_S}$ indicated by the plot's title. As network size increases, crosstalk variance decreases and theoretical approximations in Equation III A become more accurate to tightly match the simulations. Note that as expected, the capacity scales according to the minimum of d_S and d_A .

of pattern order but the network does not stay in each pattern for τ timesteps. Further increasing the nonlinearity to $d = 10$ recovers the desired sequence with correct order and timing.

Theoretical analysis of the capacity of the MixedNet (13) for general memory length τ is challenging due to the extended temporal interactions. We therefore consider single-step memory ($\tau = 1$), and show that even in this relatively tractable special case new complications arise relative to our analysis of the DenseNet. Alternatively, we can interpret the MixedNet with $\tau = 1$ as an imperfectly-learned DenseNet. If one imagines the network learns its weights through a temporally asymmetric Hebbian rule with an extended plasticity kernel, and its state is not perfectly clamped to the desired transition, the DenseNet weight matrix coupling pattern ξ^μ to $\xi^{\mu+1}$ could be corrupted by coupling of pattern ξ^μ to itself.

A. Polynomial MixedNet with $\tau = 1$

We first consider the setting where both interaction functions are polynomial, $f_S(x) = x^{d_S}$ and $f_A(x) = x^{d_A}$, and refer to this network as the Polynomial MixedNet. This model is analyzed in detail in Appendix E.1. Interestingly, this model's crosstalk variance forms a bimodal distribution, as shown in Figure E.1. This complicates the analysis, but once bimodality is accounted for one can approximate the capacity using a similar argument to that of the DenseNet. We find that

$$P_T \sim \frac{(\lambda - 1)^2}{2\gamma_{d_S, d_A}} \frac{N^{\min\{d_S, d_A\}}}{\log N}, \quad P_S \sim \frac{(\lambda - 1)^2}{2(\min\{d_S, d_A\} + 1)\gamma_{d_S, d_A}} \frac{N^{\min\{d_S, d_A\}}}{\log N}, \quad (14)$$

where γ_{d_S, d_A} is a multiplicative factor defined as

$$\gamma_{d_S, d_A} = \begin{cases} (2d_S - 1)!! & , \text{ if } d_S < d_A \\ (\lambda^2 + 1)(2d_S - 1)!! + 2\lambda[(d_S - 1)!!]^2 \mathbf{1}\{d_S \text{ even}\} & , \text{ if } d_S = d_A \\ \lambda^2(2d_A - 1)!! & , \text{ if } d_S > d_A. \end{cases} \quad (15)$$

In Figure 8, we show that simulations match the theory curves well as N increases in size.

B. Exponential MixedNet with $\tau = 1$

We now consider the the exponential MixedNet, with $f_S(x) = f_A(x) = e^{(N-1)(x-1)}$. Following our approach to the polynomial MixedNet, we approximate the crosstalk distribution as a mixture of two Gaussian, which yields the

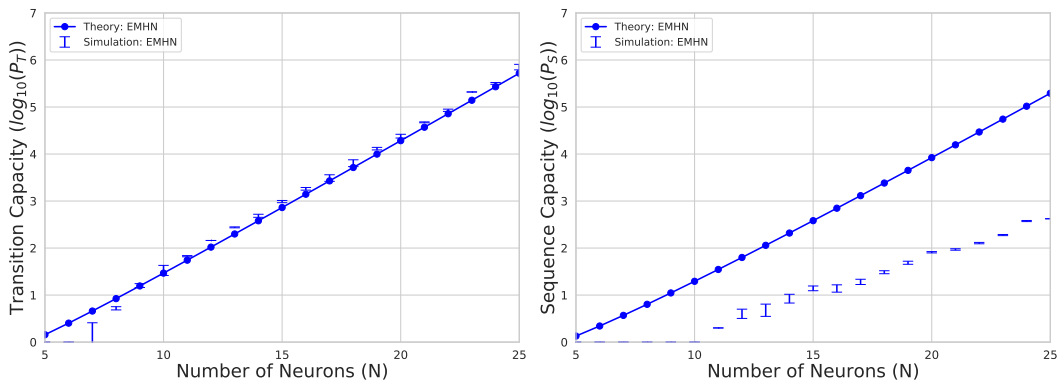


FIG. 9. The capacities of Exponential MixedNets with $\lambda = 2.5$ are plotted as a function of network size. (A) Transition capacity for the Exponential MixedNet, which closely matches theoretical prediction. The predicted capacity is shown by the solid line with dots, while square error bars show the results of numerical experiment. (B) Sequence capacity for the Exponential MixedNet, which diverges from theoretical prediction.

following predictions for the transition and sequence capacities, respectively:

$$P_T \sim \frac{(\lambda - 1)^2}{\lambda^2 + 1} \frac{\beta^{N-1}}{2 \log N} \quad \text{and} \quad P_S \sim \frac{(\lambda - 1)^2}{\lambda^2 + 1} \frac{\beta^{N-1}}{2 \log(\beta)N}, \quad \text{where} \quad \beta = \frac{\exp(2)}{\cosh(2)} \simeq 1.964 \dots \quad (16)$$

In Figure 9, we show that this Gaussian theory predicts the transition capacity of the exponential MixedNet well. However, as we observed for the exponential DenseNet, the Gaussian theory substantially overestimates the empirically measured capacity. The exponential MixedNet crosstalk distribution is subject to similar kurtosis effects as the exponential DenseNet; this deviation from Gaussianity offers a plausible explanation for the observed deviation.

IV. BIOLOGICALLY-PLAUSIBLE IMPLEMENTATION

Since biological neural networks must store sequence memories [2, 5–8], one naturally asks if these results can be generalized to biologically-plausible neural networks. A straightforward biological interpretation of the DenseNet is problematic, as a network with polynomial interaction function of degree d is equivalent to having a neural network with many-body synapses between $d + 1$ neurons. This can be seen by expanding the Polynomial DenseNet in terms of a weight tensor of $d + 1$ neurons:

$$S_i(t + 1) = \text{sgn} \left[\sum_{j_1, \dots, j_d} J_{ij_1 \dots j_d} S_{j_1}(t) \dots S_{j_d}(t) \right], \quad J_{i, j_1, \dots, j_d} = \frac{1}{N^d} \sum_{\mu=1}^P \xi_i^{\mu+1} \xi_{j_1}^\mu \dots \xi_{j_d}^\mu \quad (17)$$

This is biologically unrealistic as synaptic connections usually occur between two neurons [42]. In the case of the Exponential DenseNet, one can interpret its interaction function via a Taylor series expansion, implying synaptic connections between infinitely many neurons which is even more problematic. Similar difficulties arise in models with sum of terms with different powers [43].

To tackle this issue, we again take inspiration from earlier work in Modern Hopfield Networks. Krotov and Hopfield [44] addressed this concern for symmetric Modern Hopfield Networks by reformulating the network using two-body synapses, where the network was partitioned into a bipartite graph with visible and hidden neurons, see also [45] for an extension of this idea to deeper networks. The visible neurons correspond to the neurons in our network dynamics, \mathbf{S}_j , while the hidden neurons correspond to the individual memories stored within the network. They are connected through a weight matrix. Since we are working with an asymmetric network, we modify their approach and instead define two sets of synaptic weights: $W_{j\mu}$ connects visible neuron v_j to hidden neuron h_μ , $M_{\mu j}$ connects hidden neuron h_μ to visible neuron v_j . This results in the exact same dynamics exhibited in Equation (2), with the nonlinearity absorbed into the hidden neurons' dynamics.

For the DenseNet, we define the weights as $W_{j\mu} := \frac{1}{N} \xi_j^\mu$ and $M_{\mu j} := \xi_j^{\mu+1}$. For the MixedNet, we redefine the weight

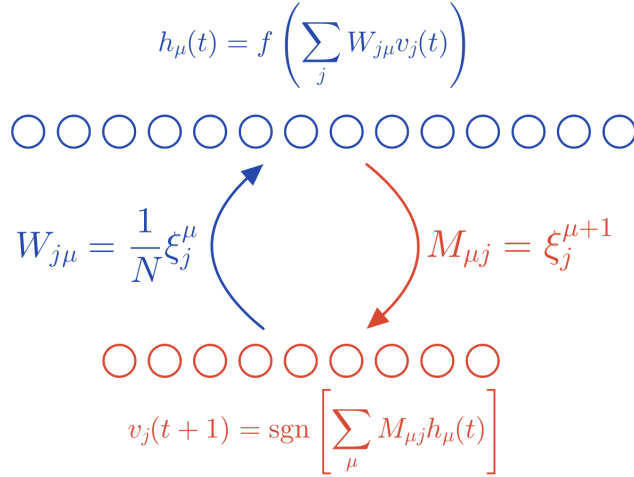


FIG. 10. Biologically-plausible implementation of the DenseNet.

matrix $M_{\mu j} = \xi_j^\mu + \lambda \xi_j^{\mu+1}$. The update rules for the neurons are given by

$$h_\mu(t) := f\left[\sum_j W_{j\mu} v_j(t)\right], \quad v_j(t+1) := \text{sgn}\left[\sum_\mu M_{\mu j} h_\mu(t)\right]. \quad (18)$$

Note that these networks' transition and sequence capacities, P_T and P_S , now scale linearly with respect to the total number of neurons in this model, N visible neurons and P hidden neurons. However, the network capacity still scales nonlinearly with respect to the number of visible neurons.

Finally, we note that this network is reminiscent of recent computational models for motor action selection and control via the cortico-basal ganglia-thalamo-cortical loop, in which the basal ganglia inhibits thalamic neurons that are bidirectionally connected to a recurrent cortical network [5, 46]. This relates to our model as follows: the motor cortex (visible neurons) executes an action, each thalamic unit (hidden neurons) encodes a motor motif, and the basal ganglia silences thalamic neurons (external network modulating context). In particular, the role of the basal ganglia in this network suggests a novel mechanism of context-dependent gating within Hopfield Networks [47]. Rather than modulating synapses or feature neurons in a network, one can directly inhibit (activate) memory neurons in order to decrease (increase) the likelihood of transitioning to the associated state. Similarly, thalamocortical loops have been found to be important to song generation in zebra finches [48]. Thus, the biological implementation of the DenseNet can provide insight into how biological agents reliably store and generate complex sequences.

V. DISCUSSION AND FUTURE DIRECTIONS

We introduced the DenseNet for the reliable storage and recall of long sequences of patterns, derived the scaling of its single-transition and full-sequence capacity, and verified these results in numerical simulation. We found that depending on the choice of nonlinear interaction function, the DenseNet could scale polynomially or exponentially. For small Exponential DenseNets, we see that the crosstalk distribution is highly kurtotic, leading to significant deviation between simulation and theoretical results derived in the thermodynamic limit.

We have also tested the ability of these models to recall sequences of correlated patterns, by comparing the storage and recall of a sequence of MNIST images with different nonlinearities. As expected, the network's reconstruction capabilities increased with the nonlinearity power d . The best results are achieved with the exponential nonlinearity. To further increase the capacity, we have introduced the generalized pseudoinverse rule and demonstrated in simulation its ability to maintain high capacity for highly correlated patterns. We have also introduced and analyzed MixedNet, containing both symmetric and asymmetric terms, to maintain patterns within sequences for longer periods of time.

While we have utilized a generalization of the fixed-point capacity for sequence memory, this is not the only notion of capacity one could consider. In other studies of MHNs, instead of considering stability as the probability of staying at a fixed point, researchers quantify the probability that the network will reach a fixed point within a single transition [30, 49, 50]. This approach allows one to quantify noise-robustness and the size of each memory's basin of attraction

[35]. More broadly, one could consider other definitions of associative memory capacity not addressed here, including those that depend only on network architecture and not on the assumption of a particular learning rule [51, 52]. However, as compared to the relatively simple analysis that is possible for the fixed-point capacity of a Hopfield network using a Hebbian learning rule, analyzing these alternative notions of capacity in nonlinear networks can pose significant technical challenges [52–54].

There has been a renewed interest in storing sequences of memories not just within biological systems. Steinberg and Sompolinsky [55] proposed a novel approach to store sequences in Hopfield networks. By using vector-symbolic architectures to bind each pattern to its temporal order in the sequence, the network can store an entire sequence as a single attractor. However, this model suffers from the same capacity issues as the Hopfield Network, and could be extended using nonlinear interaction functions for better capacity and more robust recall. Herron *et al.* [56] investigated an alternative mechanism for robust sequence recall within complex systems more broadly. Instead of modulating the input into neurons, they propose a way to reduce crosstalk by directly modulating interactions between neurons.

In this work, we limited ourselves to theoretical analysis of discrete-time networks storing binary patterns. An important direction for future research would be to go beyond the Gaussian theory in order to develop accurate predictions of the Exponential DenseNet capacity. There are also many potential avenues for extending these models and methods, including to continuous-time networks, continuous-valued patterns, computing capacity for correlated patterns, testing different weight functions, and examining different network topologies.

ACKNOWLEDGMENTS

We thank Matthew Farrell, Shanshan Qin, and Sabarish Sainathan for useful discussions and comments on earlier versions of our manuscript. HC was supported by the GFSD Fellowship. JAZ-V and CP were supported by NSF Award DMS-2134157. The computations in this paper were run on the FASRC Cannon cluster supported by the FAS Division of Science Research Computing Group at Harvard University.

-
- [1] D. Kleinfeld and H. Sompolinsky, Associative neural network model for the generation of temporal patterns. theory and application to central pattern generators, *Biophysical Journal* **54**, 1039 (1988).
 - [2] M. A. Long, D. Z. Jin, and M. S. Fee, Support for a synaptic chain model of neuronal sequence generation, *Nature* **468**, 394 (2010).
 - [3] M. Gillett, U. Pereira, and N. Brunel, Characteristics of sequential activity in networks with temporally asymmetric Hebbian learning, *Proceedings of the National Academy of Sciences* **117**, 29948 (2020).
 - [4] S. Recanatesi, U. Pereira-Obilinovic, M. Murakami, Z. Mainen, and L. Mazzucato, Metastable attractors explain the variable timing of stable behavioral action sequences, *Neuron* **110**, 139 (2022).
 - [5] L. Mazzucato, Neural mechanisms underlying the temporal organization of naturalistic animal behavior, *eLife* **11**, e76577 (2022).
 - [6] E. T. Rolls and P. Mills, The generation of time in the hippocampal memory system, *Cell Reports* **28**, 1649 (2019).
 - [7] A. Wiltschko, M. Johnson, G. Iurilli, R. Peterson, J. Katon, S. Pashkovski, V. Abaira, R. Adams, and S. Datta, Mapping sub-second structure in mouse behavior, *Neuron* **88**, 1121 (2015).
 - [8] J. E. Markowitz, W. F. Gillis, M. Jay, J. Wood, R. W. Harris, R. Cieszkowski, R. Scott, D. Brann, D. Koveal, T. Kula, C. Weinreb, M. A. M. Osman, S. R. Pinto, N. Uchida, S. W. Linderman, B. L. Sabatini, and S. R. Datta, Spontaneous behaviour is structured by reinforcement without explicit reward, *Nature* **614**, 108 (2023).
 - [9] C. Pehlevan, F. Ali, and B. P. Ölveczky, Flexibility in motor timing constrains the topology and dynamics of pattern generator circuits, *Nature communications* **9**, 977 (2018).
 - [10] H. Sompolinsky and I. Kanter, Temporal Association in Asymmetric Neural Networks, *Physical Review Letters* **57**, 2861 (1986).
 - [11] Z. Jiang, Z. Chen, T. Hou, and H. Huang, Spectrum of non-Hermitian deep-Hebbian neural networks, *Physical Review Research* **5**, 013090 (2023).
 - [12] U. Pereira and N. Brunel, Unsupervised learning of persistent and sequential activity, *Frontiers in Computational Neuroscience* **13**, 97 (2020).
 - [13] C. Leibold and R. Kempter, Memory capacity for sequences in a recurrent network with biological constraints, *Neural Computation* **18**, 904 (2006).
 - [14] J. Hawkins, D. George, and J. Niemasik, Sequence memory for prediction, inference and behaviour, *Philosophical Transactions of the Royal Society B: Biological Sciences* **364**, 1203 (2009).
 - [15] J. Hawkins and S. Ahmad, Why neurons have thousands of synapses, a theory of sequence memory in neocortex, *Frontiers in Neural Circuits* , 23 (2016).
 - [16] D. J. Amit, Neural networks counting chimes, *Proceedings of the National Academy of Sciences* **85**, 2141 (1988).
 - [17] H. Gutfreund and M. Mezard, Processing of temporal sequences in neural networks, *Phys. Rev. Lett.* **61**, 235 (1988).

- [18] K. Rajan, C. Harvey, and D. Tank, Recurrent network models of sequence generation and memory, *Neuron* **90**, 128 (2016).
- [19] M. Diesmann, M.-O. Gewaltig, and A. Aertsen, Stable propagation of synchronous spiking in cortical neural networks, *Nature* **402**, 529 (1999).
- [20] N. F. Hardy and D. V. Buonomano, Neurocomputational models of interval and pattern timing, *Current Opinion in Behavioral Sciences* **8**, 250 (2016), time in perception and action.
- [21] D. Obeid, J. A. Zavatone-Veth, and C. Pehlevan, Statistical structure of the trial-to-trial timing variability in synfire chains, *Phys. Rev. E* **102**, 052406 (2020).
- [22] S.-I. Amari, Learning patterns and pattern sequences by self-organizing nets of threshold elements, *IEEE Transactions on computers* **100**, 1197 (1972).
- [23] J. J. Hopfield, Neural networks and physical systems with emergent collective computational abilities., *Proceedings of the National Academy of Sciences* **79**, 2554 (1982).
- [24] J. J. Hopfield, Neurons with graded response have collective computational properties like those of two-state neurons., *Proceedings of the national academy of sciences* **81**, 3088 (1984).
- [25] J. Hertz, A. Krogh, and R. G. Palmer, *Introduction to the theory of neural computation* (CRC Press, 2018).
- [26] D. J. Amit, H. Gutfreund, and H. Sompolinsky, Spin-glass models of neural networks, *Physical Review A* **32**, 1007 (1985).
- [27] D. J. Amit, H. Gutfreund, and H. Sompolinsky, Storing infinite numbers of patterns in a spin-glass model of neural networks, *Phys. Rev. Lett.* **55**, 1530 (1985).
- [28] D. J. Amit, H. Gutfreund, and H. Sompolinsky, Statistical mechanics of neural networks near saturation, *Annals of Physics* **173**, 30 (1987).
- [29] D. Krotov and J. J. Hopfield, Dense associative memory for pattern recognition, *Advances in Neural Information Processing Systems* **29** (2016).
- [30] M. Demircigil, J. Heusel, M. Löwe, S. Uppang, and F. Vermet, On a model of associative memory with huge storage capacity, *Journal of Statistical Physics* **168**, 288 (2017), arXiv:1702.01929 [math].
- [31] D. Krotov, A new frontier for hopfield networks, *Nature Reviews Physics* , 1 (2023).
- [32] A. Karuvally, T. J. Sejnowski, and H. T. Siegelmann, Energy-based general sequential episodic memory networks at the adiabatic limit, arXiv preprint arXiv:2212.05563 (2022).
- [33] D. Petritis, Thermodynamic formalism of neural computing, in *Dynamics of Complex Interacting Systems*, edited by E. Goles and S. Martínez (Springer Netherlands, Dordrecht, 1996) pp. 81–146.
- [34] A. Bovier, Sharp upper bounds on perfect retrieval in the Hopfield model, *Journal of Applied Probability* **36**, 941–950 (1999).
- [35] R. McEliece, E. Posner, E. Rodemich, and S. Venkatesh, The capacity of the Hopfield associative memory, *IEEE Transactions on Information Theory* **33**, 461 (1987).
- [36] G. Weisbuch and F. Fogelman-Soulié, Scaling laws for the attractors of Hopfield networks, *J. Physique Lett.* **46**, 623 (1985).
- [37] V. V. Petrov, *Sums of Independent Random Variables* (De Gruyter, Berlin, Boston, 1975) trans. A. A. Brown.
- [38] J. E. Kolassa, *Series Approximation Methods in Statistics* (Springer New York, 1997).
- [39] J. E. Kolassa and P. McCullagh, Edgeworth Series for Lattice Distributions, *The Annals of Statistics* **18**, 981 (1990).
- [40] D. Dolgopyat and K. Fernando, An Error Term in the Central Limit Theorem for Sums of Discrete Random Variables, *International Mathematics Research Notices* **10.1093/imrn/rnad088** (2023), rnad088.
- [41] I. Kanter and H. Sompolinsky, Associative recall of memory without errors, *Phys. Rev. A* **35**, 380 (1987).
- [42] E. R. Kandel, J. H. Schwartz, T. M. Jessell, S. Siegelbaum, A. J. Hudspeth, S. Mack, *et al.*, *Principles of neural science*, 6th ed. (McGraw-hill New York, 2021).
- [43] T. F. Burns and T. Fukai, Simplicial Hopfield networks, in *The Eleventh International Conference on Learning Representations* (2023).
- [44] D. Krotov and J. J. Hopfield, Large associative memory problem in neurobiology and machine learning, in *International Conference on Learning Representations* (2021).
- [45] D. Krotov, Hierarchical associative memory, arXiv preprint arXiv:2107.06446 (2021).
- [46] L. Loggiaco, L. Abbott, and S. Escola, Thalamic control of cortical dynamics in a model of flexible motor sequencing, *Cell Reports* **35**, 109090 (2021).
- [47] N. Y. Masse, G. D. Grant, and D. J. Freedman, Alleviating catastrophic forgetting using context-dependent gating and synaptic stabilization, *Proceedings of the National Academy of Sciences* **115**, 10.1073/pnas.1803839115 (2018), arXiv:1802.01569 [cs, q-bio].
- [48] F. W. Moll, D. Kranz, A. Corredera Asensio, M. Elmaleh, L. A. Ackert-Smith, and M. A. Long, Thalamus drives vocal onsets in the zebra finch courtship song, *Nature* **616**, 132 (2023).
- [49] H. Ramsauer, B. Schäffl, J. Lehner, P. Seidl, M. Widrich, L. Gruber, M. Holzleitner, T. Adler, D. Kreil, M. K. Kopp, G. Klambauer, J. Brandstetter, and S. Hochreiter, Hopfield networks is all you need, in *International Conference on Learning Representations* (2021).
- [50] C. Lucibello and M. Mézard, The exponential capacity of dense associative memories, arXiv preprint arXiv:2304.14964 (2023).
- [51] A. Knoblauch, G. Palm, and F. T. Sommer, Memory capacities for synaptic and structural plasticity, *Neural Computation* **22**, 289 (2010).
- [52] J. A. Zavatone-Veth and C. Pehlevan, On neural network kernels and the storage capacity problem, *Neural Computation* **34**, 1136 (2022).
- [53] J. A. Zavatone-Veth and C. Pehlevan, Activation function dependence of the storage capacity of treelike neural networks, *Phys. Rev. E* **103**, L020301 (2021).

- [54] R. Monasson and R. Zecchina, Weight space structure and internal representations: A direct approach to learning and generalization in multilayer neural networks, *Phys. Rev. Lett.* **75**, 2432 (1995).
- [55] J. Steinberg and H. Sompolinsky, Associative memory of structured knowledge, *Scientific Reports* **12**, 21808 (2022).
- [56] L. Herron, P. Sartori, and B. Xue, Robust retrieval of dynamic sequences through interaction modulation, arXiv preprint arXiv:2211.17152 (2022).
- [57] H. Chen, Y. Lee, G. Sun, H. Lee, T. Maxwell, and C. L. Giles, High order correlation model for associative memory, in *AIP Conference Proceedings*, Vol. 151 (American Institute of Physics, 1986) pp. 86–99.
- [58] D. Psaltis and C. H. Park, Nonlinear discriminant functions and associative memories, in *AIP conference Proceedings*, Vol. 151 (American Institute of Physics, 1986) pp. 370–375.
- [59] P. Baldi and S. S. Venkatesh, Number of stable points for spin-glasses and neural networks of higher orders, *Physical Review Letters* **58**, 913 (1987).
- [60] E. Gardner, Multiconnected neural network models, *Journal of Physics A: Mathematical and General* **20**, 3453 (1987).
- [61] L. F. Abbott and Y. Arian, Storage capacity of generalized networks, *Physical review A* **36**, 5091 (1987).
- [62] D. Horn and M. Usher, Capacities of multiconnected memory models, *Journal de Physique* **49**, 389 (1988).
- [63] E. Agliari, A. Fachechi, and C. Marullo, Nonlinear PDEs approach to statistical mechanics of dense associative memories, *Journal of Mathematical Physics* **63**, 103304 (2022).
- [64] E. Agliari, L. Albanese, F. Alemanno, A. Alessandrelli, A. Barra, F. Giannotti, D. Lotito, and D. Pedreschi, Dense Hebbian neural networks: a replica symmetric picture of unsupervised learning, arXiv [10.48550/ARXIV.2211.14067](https://arxiv.org/abs/10.48550/ARXIV.2211.14067) (2022).
- [65] L. Albanese, F. Alemanno, A. Alessandrelli, and A. Barra, Replica symmetry breaking in dense Hebbian neural networks, *Journal of Statistical Physics* **189**, 24 (2022).
- [66] DLMF, *NIST Digital Library of Mathematical Functions*, <http://dlmf.nist.gov/>, Release 1.1.1 of 2021-03-15 (2021), f. W. J. Olver, A. B. Olde Daalhuis, D. W. Lozier, B. I. Schneider, R. F. Boisvert, C. W. Clark, B. R. Miller, B. V. Saunders, H. S. Cohl, and M. A. McClain, eds.
- [67] Y. LeCun, C. Cortes, and C. Burges, MNIST handwritten digit database, *ATT Labs [Online]* **2** (2010).

Appendix A: Review of Modern Hopfield Networks

Here we review the Hopfield network and its modern generalization as an auto-associative memory model. These ideas will be helpful for storing sequences in network dynamics.

1. The Hopfield Network

We first introduce the classic Hopfield Network [23]. Let N be the number of neurons in the network and $\mathbf{S}(t) \in \{-1, +1\}^N$ be the state of the network at time t . The task is to store P patterns, $\{\boldsymbol{\xi}^1, \dots, \boldsymbol{\xi}^P\}$, where $\xi_j^\mu \in \{\pm 1\}$ is the j^{th} neuron of the μ^{th} pattern. The goal is to design a network with dynamics such that when the network is initialized with a pattern, it will converge to one of the stored memories.

The Hopfield Network [23] attempts this by following the discrete-time synchronous update rule⁴:

$$\mathbf{S}(t+1) = \mathbf{T}_{HN}(\mathbf{S}(t)), \quad (\text{A.1})$$

where the transition operator $T_{HN}(\cdot)_i$ for neuron i is defined in terms of symmetric Hebbian weights:

$$T_{HN}(\mathbf{S})_i = \text{sgn} \left[\sum_{j \neq i} J_{ij} S_j \right], \quad J_{ij} = \frac{1}{N} \sum_{\mu=1}^P \xi_i^\mu \xi_j^\mu. \quad (\text{A.2})$$

Note that we are excluding self-interaction terms (J_{ii}) in Equation A.2. To interpret this dynamics from another useful point of view, we define the overlap, or Mattis magnetization, m_i^μ of the network state \mathbf{S} with pattern $\boldsymbol{\xi}^\mu$. We can then rewrite the update rule for the Hopfield Network as

$$T_{HN}(\mathbf{S})_i := \text{sgn} \left[\sum_{\mu=1}^P \xi_i^\mu m_i^\mu \right], \quad m_i^\mu := \frac{1}{(N-1)} \sum_{j \neq i} \xi_j^\mu S_j \quad (\text{A.3})$$

We interpret this as at every time t , the network tries to identify the pattern $\boldsymbol{\xi}^\mu$ it is closest to and updates neuron i to the value for that pattern. A natural question to ask about the associative memory networks is their capacity: how many patterns can be stored and recalled with minimal error? This question has been the subject of many studies [23, 26–28, 33–36]. Intuitively, in recalling a pattern $\boldsymbol{\xi}^\nu$, what limits the network’s capacity is the overlap between the pattern $\boldsymbol{\xi}^\nu$ and other patterns, referred to as the crosstalk [25, 36].

A precise answer to the storage capacity question can be given under the assumption that the patterns $\{\boldsymbol{\xi}^\mu\}$ are sampled from some probability distribution. While different notions of capacity have been considered in the literature [23, 26–28, 33–36], we focus on the *fixed-point capacity*, which characterizes the probability that, when initialized at a given pattern, the network dynamics do not move the state away from that point. To render the problem analytically tractable, it is usually assumed that the pattern components are i.i.d. Rademacher random variables, i.e., $\mathbb{P}(\xi_j^\mu = \pm 1) = 1/2$ for all j and μ . Then, at finite network size one can define the capacity as

$$P_{HN}(N, c) = \max \{ P \in \{2, \dots, 2^N\} : \mathbb{P} [\cap_{\mu=1}^P \{ \mathbf{T}_{HN}(\boldsymbol{\xi}^\mu) = \boldsymbol{\xi}^\mu \}] \geq 1 - c \}, \quad (\text{A.4})$$

where $c \in [0, 1)$ is a fixed error tolerance. As we review in detail in Appendix B, one finds an asymptotic capacity estimate $P_{HN} \sim \frac{N}{4 \log(N)}$ for $c = 0$, which can be shown to be a sharp threshold [33–35].

2. Modern Hopfield Networks

Recent work from Krotov and Hopfield [29] reinvigorated a line of research into generalized Hopfield Networks with larger capacity [57–62], resulting in what are now called Dense Associative Memories or Modern Hopfield Networks:

$$T_{MHN}(\mathbf{S})_i := \text{sgn} \left[\sum_{\mu=1}^P \xi_i^\mu f(m_i^\mu) \right] \quad (\text{A.5})$$

⁴ For the Hopfield network, one can also consider an asynchronous update rule in which only one neuron is updated at each timestep [23, 25].

where f , referred to as the interaction function, is a nonlinear monotonically increasing function whose purpose is to separate the pattern overlaps for better signal to noise ratio. Since $m_i^\mu(t)$ has a maximum value of 1, this means contributions from patterns with partial overlaps will be reduced by the interaction function. This diminishes the crosstalk and thereby increases the probability of transitioning to the correct pattern. If the interaction function is chosen to be $f(x) = x^d$, then the MHN's capacity has been shown to scale polynomially with network size as $P \sim \beta_d \frac{N^d}{\log(N)}$, where β_d is a numerical constant depending on the degree d [29, 63–65]. Using a different definition of capacity, Demircigil *et al.* [30] have also shown that an exponential nonlinearity can lead to exponential scaling of the capacity. See [31] for a recent review of these results.

Appendix B: Review of Hopfield network fixed-point capacity

In this Appendix, we review the computation of the classical Hopfield network fixed-point capacity. Our approach will follow—but not exactly match—that of Petritis [33]. Though these results are standard, we review them in detail both because this approach will inspire in part our approach to the DenseNet, and because several important steps of the analysis are significantly simpler than the corresponding steps for the DenseNet.

We begin by recalling that the Hopfield network update can be written as

$$T_{HN}(\mathbf{S})_i := \text{sgn} \left[\sum_{\mu=1}^P \xi_i^\mu \left(\frac{1}{N-1} \sum_{j \neq i} \xi_j^\mu S_j \right) \right], \quad (\text{B.1})$$

and that our goal is to determine

$$P_{HN}(N, c) = \max \{ P \in \{2, \dots, 2^N\} : \mathbb{P} [\cap_{\mu=1}^P \{\mathbf{T}_{HN}(\boldsymbol{\xi}^\mu) = \boldsymbol{\xi}^\mu\}] \geq 1 - c \} \quad (\text{B.2})$$

for some absolute constant $0 \leq c < 1$, at least in the regime where $N, P \gg 1$ [33–36]. As is standard in theoretical studies of Hopfield model capacity [25–28, 33–36], we take in these probabilities the pattern components ξ_k^μ to be independent and identically distributed Rademacher random variables. We can expand the memorization probability as a union of single-bitflip events:

$$\mathbb{P} \left[\bigcap_{\mu=1}^P \{\mathbf{T}_{HN}(\boldsymbol{\xi}^\mu) = \boldsymbol{\xi}^\mu\} \right] = 1 - \mathbb{P} \left[\bigcup_{\mu=1}^P \bigcup_{i=1}^N \{T_{HN}(\boldsymbol{\xi}^\mu)_i \neq \xi_i^\mu\} \right]. \quad (\text{B.3})$$

This illustrates why analyzing the memorization probability is complicated: the single-pattern events $\mathbf{T}_{HN}(\boldsymbol{\xi}^\mu) = \boldsymbol{\xi}^\mu$ are not independent across patterns μ , and each single-pattern event is itself the intersection of non-independent single-neuron events $T_{HN}(\boldsymbol{\xi}^\mu)_i = \xi_i^\mu$. However, as the single-bitflip probabilities $\mathbb{P}[T_{HN}(\boldsymbol{\xi}^\mu)_j \neq \xi_j^\mu]$ are identical for all μ and j , we can obtain a straightforward union bound

$$\mathbb{P} \left[\bigcap_{\mu=1}^P \{\mathbf{T}_{HN}(\boldsymbol{\xi}^\mu) = \boldsymbol{\xi}^\mu\} \right] = 1 - \mathbb{P} \left[\bigcup_{\mu=1}^P \bigcup_{i=1}^N \{T_{HN}(\boldsymbol{\xi}^\mu)_i \neq \xi_i^\mu\} \right] \quad (\text{B.4})$$

$$\geq 1 - \sum_{\mu=1}^P \sum_{i=1}^N \mathbb{P}[T_{HN}(\boldsymbol{\xi}^\mu)_i \neq \xi_i^\mu] \quad (\text{B.5})$$

$$= 1 - NP \mathbb{P}[T_{HN}(\boldsymbol{\xi}^1)_1 \neq \xi_1^1], \quad (\text{B.6})$$

where we focus without loss of generality on the first element of the first pattern. Therefore, if we can control the single-bitflip probability $\mathbb{P}[T_{HN}(\boldsymbol{\xi}^1)_1 \neq \xi_1^1]$, we can obtain a lower bound on the true capacity. In particular,

$$P_{HN}(N, c) \geq \max \{ P \in \{2, \dots, 2^N\} : NP \mathbb{P}[T_{HN}(\boldsymbol{\xi}^1)_1 \neq \xi_1^1] \leq c \} \quad (\text{B.7})$$

From the definition of the Hopfield network update rule, we have

$$\mathbb{P}[T_{HN}(\boldsymbol{\xi}^1)_1 \neq \xi_1^1] = \mathbb{P} \left\{ \text{sgn} \left[\frac{1}{N-1} \sum_{\mu=1}^P \sum_{j \neq i} \xi_1^\mu \xi_j^\mu \xi_j^1 \right] \neq \xi_1^1 \right\} \quad (\text{B.8})$$

$$= \mathbb{P} \left[\frac{1}{N-1} \sum_{\mu=1}^P \sum_{j \neq i} \xi_1^1 \xi_1^\mu \xi_j^1 \xi_j^\mu < 0 \right] \quad (\text{B.9})$$

$$= \mathbb{P}[C > 1], \quad (\text{B.10})$$

where we have defined

$$C = \frac{1}{N-1} \sum_{\mu=2}^P \sum_{j \neq i} \xi_1^1 \xi_1^\mu \xi_j^1 \xi_j^\mu \quad (\text{B.11})$$

and used the fact that the distribution of C is symmetric. C is referred to as the *crosstalk*, because it represents the effect of interference between the first pattern and the other $P-1$ patterns on recall of the first pattern. We can simplify the crosstalk using the fact that, since we have assumed i.i.d. Rademacher patterns, we have the equality in distribution

$$\xi_j^1 \xi_j^\mu \stackrel{d}{=} \xi_j^\mu \quad (\text{B.12})$$

for all $\mu = 2, \dots, P$ and $j = 1, \dots, N$, yielding

$$C \stackrel{d}{=} \frac{1}{N-1} \sum_{\mu=2}^P \sum_{j \neq i} \xi_1^\mu \xi_j^\mu. \quad (\text{B.13})$$

Similarly, we have

$$\xi_1^\mu \xi_j^\mu \stackrel{d}{=} \xi_j^\mu \quad (\text{B.14})$$

for all $\mu = 2, \dots, P$ and $j = 2, \dots, N$, which finally yields

$$C \stackrel{d}{=} \frac{1}{N-1} \sum_{\mu=2}^P \sum_{j \neq i} \xi_j^\mu. \quad (\text{B.15})$$

Therefore, for the classic Hopfield network the crosstalk is equal in distribution to the sum of $(P-1)(N-1)$ i.i.d. Rademacher random variables.

1. Approach 1: Hoeffding's inequality

Now, we can immediately apply Hoeffding's inequality, which implies that for any $t > 0$

$$\mathbb{P} \left[\sum_{\mu=2}^P \sum_{k=2}^N \xi_k^\mu > t \right] \leq \exp \left(-\frac{1}{2} \frac{t^2}{(P-1)(N-1)} \right). \quad (\text{B.16})$$

We then have that

$$\mathbb{P} \left[\sum_{\mu=2}^P \sum_{k=2}^N \xi_k^\mu > N-1 \right] \leq \exp \left(-\frac{1}{2} \frac{N-1}{P-1} \right). \quad (\text{B.17})$$

We then have the bound

$$P_{HN}(N, c) \geq \max \left\{ P \in \{2, \dots, 2^N\} : NP \exp \left(-\frac{1}{2} \frac{N-1}{P-1} \right) \leq c \right\}. \quad (\text{B.18})$$

We now want to consider the regime $N \gg 1$, and demand that the error probability should tend to zero as we increase N . If we substitute in the *Ansatz*

$$P \sim \frac{N}{\alpha \log N}, \quad (\text{B.19})$$

the bound is easily seen to tend to zero for all $\alpha \geq 4$, yielding an estimated capacity of

$$P_{HN} \sim \frac{N}{4 \log N}. \quad (\text{B.20})$$

As this estimates follows from a sequence of lower bounds on the memorization probability, it is a lower bound on the true capacity of the model [33]. However, via a more involved argument that accounts for the associations between the events $\mathbf{T}_{HN}(\boldsymbol{\xi}^\mu) = \boldsymbol{\xi}^\mu$, it was shown by Bovier [34] to be tight.

For the classical Hopfield network, the single bitflip probability $\mathbb{P}[C > 1]$ is easy to control using elementary concentration inequalities because the crosstalk can be expressed as a sum of $(P-1)(N-1)$ i.i.d. random variables. Therefore, we expect the crosstalk to concentrate whenever N or P or both together are large. However, for the DenseNet, we will find in Appendix C that the crosstalk is given as the sum of $P-1$ i.i.d. random variables, each of which is a nonlinear function applied to the sum of $N-1$ i.i.d. Rademacher random variables. Naïve application of Hoeffding's inequality is then not particularly useful. We will therefore take a simpler, though less rigorously controlled approach, which can also be applied to the classical Hopfield network: we approximate the distribution of the crosstalk as Gaussian [25].

2. Approach 2: Gaussian approximation

For the classical Hopfield network, the fact that the crosstalk can be expressed as a sum of $(P-1)(N-1)$ i.i.d. Rademacher random variables means that the classical central limit theorem implies that it tends in distribution to a Gaussian whenever $(P-1)(N-1)$ tends to infinity. By symmetry, the mean of the crosstalk is zero, while its variance is easily seen to be

$$\text{var}(C) = \frac{P-1}{N-1}. \quad (\text{B.21})$$

If we approximate the distribution of the crosstalk for N and P large but finite by a Gaussian, we therefore have

$$\mathbb{P}[C > 1] \approx H\left(\sqrt{\frac{N-1}{P-1}}\right) \quad (\text{B.22})$$

where $H(x) = \text{erfc}(x/\sqrt{2})/2$ is the Gaussian tail distribution function. We want to have $\mathbb{P}[C > 1] \rightarrow 0$, so we must have $(P-1)/(N-1) \rightarrow 0$. Then, we can use the asymptotic expansion [25]

$$H(\sqrt{z}) = \frac{1}{\sqrt{2\pi z}} \exp\left(-\frac{z}{2}\right) \left[1 + \mathcal{O}\left(\frac{1}{z}\right)\right] \quad \text{as } z \rightarrow \infty \quad (\text{B.23})$$

to obtain the heuristic Gaussian approximation

$$\mathbb{P}[C > 1] \approx \sqrt{\frac{(P-1)}{2\pi(N-1)}} \exp\left(-\frac{(N-1)}{2(P-1)}\right). \quad (\text{B.24})$$

If we use this Gaussian approximation instead of the Hoeffding bound applied above, we can easily see that we will obtain identical estimates for the capacity with an error tolerance tending to zero. However, we have given up the rigor of the bound from Hoeffding's inequality, since we have not controlled the rate of convergence to the Gaussian tail probability. In particular, the Berry-Esseen theorem would give in this case a uniform additive error bound of $1/\sqrt{(P-1)(N-1)}$, which in the regime $P \sim N/[\alpha \log N]$ cannot compete with the factors of N or NP which we want $\mathbb{P}[C > 1]$ to overwhelm. We will not worry about this issue, as we are concerned more with whether we can get accurate capacity estimates that match numerical experiment than whether we can prove those estimates completely rigorously.

We can also use the Gaussian approximation to estimate the capacity for a non-zero error threshold c at finite N . Concretely, if we demand that the union bound is saturated, i.e.,

$$NP \mathbb{P}[T_{HN}(\boldsymbol{\xi}^1)_1 \neq \xi_1^1] = c, \quad (\text{B.25})$$

under the Gaussian approximation for the bitflip probability we have the self-consistent equation

$$NPH\left(\sqrt{\frac{N-1}{P-1}}\right) = c \quad (\text{B.26})$$

for P , which we can re-write as

$$P-1 = \frac{N-1}{[H^{-1}(c/NP)]^2}. \quad (\text{B.27})$$

This is a transcendental self-consistent equation, which is not easy to solve analytically. However, we can make some progress at small $c/(NP)$. Using the asymptotic expansion of the inverse of the complementary error function [66], we have

$$[H^{-1}(x)]^2 = 2 \operatorname{inverfc}(2x)^2 \quad (\text{B.28})$$

$$\sim -\log \left[4\pi x^2 \log \left(\frac{1}{2x} \right) \right] \quad (\text{B.29})$$

$$= -2 \log(x) - \log(4\pi) - \log \log \left(\frac{1}{2x} \right) \quad (\text{B.30})$$

$$\sim -2 \log(x) \quad (\text{B.31})$$

as $x \rightarrow 0$. Then, assuming c is such that $-\log(c)$ is negligible relative to $\log(NP)$, we have

$$P \sim \frac{N}{2 \log(NP)}, \quad (\text{B.32})$$

which we can solve for P as

$$P \sim \frac{N}{2W_0(N^2/2)}, \quad (\text{B.33})$$

where W_0 is the principal branch of the Lambert- W function [66]. But, at large N , we can use the asymptotic $W_0(N) \sim \log(N)$ to obtain the approximate scaling

$$P \sim \frac{N}{4 \log(N)}, \quad (\text{B.34})$$

which agrees with our earlier result. Conceptually, this intuition is consistent with there being a sharp transition in the thermodynamic limit, as proved rigorously by Bovier [34].

Appendix C: DenseNet Capacity

In this Appendix, we analyze the capacity of the DenseNet. As introduced in Section II A of the main text, there are two notions of robustness to consider: the robustness of a single transition and the robustness of the full sequence. For a fixed $N \in \{2, 3, \dots\}$ and an error tolerance $c \in [0, 1)$, we define these two notions of capacity as

$$P_T(N, c) = \max \{P \in \{2, \dots, 2^N\} : \mathbb{P}[\mathbf{T}_{DN}(\boldsymbol{\xi}^1) = \boldsymbol{\xi}^2] \geq 1 - c\} \quad (\text{C.1})$$

and

$$P_S(N, c) = \max \{P \in \{2, \dots, 2^N\} : \mathbb{P}[\cap_{\mu=1}^P \{\mathbf{T}_{DN}(\boldsymbol{\xi}^\mu) = \boldsymbol{\xi}^{\mu+1}\}] \geq 1 - c\}, \quad (\text{C.2})$$

respectively.

Our goal is to approximately compute the capacity in the regime in which N and P are large. Following Petritis [33]'s approach to the HN, to make analytical progress, we can use a union bound to control the single-step error probability in terms of the probability of a single bitflip:

$$\begin{aligned} & \mathbb{P}[\mathbf{T}_{DN}(\boldsymbol{\xi}^\mu) = \boldsymbol{\xi}^{\mu+1}] \\ &= 1 - \mathbb{P} \left[\bigcup_{i=1}^N \{T_{DN}(\boldsymbol{\xi}^\mu)_i \neq \xi_i^{\mu+1}\} \right] \end{aligned} \quad (\text{C.3})$$

$$\geq 1 - \sum_{i=1}^N \mathbb{P} [T_{DN}(\boldsymbol{\xi}^\mu)_i \neq \xi_i^{\mu+1}] \quad (\text{C.4})$$

$$= 1 - N \mathbb{P}[T_{DN}(\boldsymbol{\xi}^1)_1 \neq \xi_2^1]. \quad (\text{C.5})$$

where we use the fact that all elements of all patterns are i.i.d. by assumption. We use a similar approach to control the sequence error probability in terms of the probability of a single bitflip:

$$\begin{aligned} & \mathbb{P} \left[\bigcap_{\mu=1}^P \{ \mathbf{T}_{DN}(\boldsymbol{\xi}^\mu) = \boldsymbol{\xi}^{\mu+1} \} \right] \\ &= 1 - \mathbb{P} \left[\bigcup_{\mu=1}^P \bigcup_{i=1}^N \{ T_{DN}(\boldsymbol{\xi}^\mu)_i \neq \xi_i^{\mu+1} \} \right] \end{aligned} \quad (\text{C.6})$$

$$\geq 1 - \sum_{\mu=1}^P \sum_{i=1}^N \mathbb{P} \left[T_{DN}(\boldsymbol{\xi}^\mu)_i \neq \xi_i^{\mu+1} \right] \quad (\text{C.7})$$

$$= 1 - NP \mathbb{P}[T_{DN}(\boldsymbol{\xi}^1)_1 \neq \xi_2^1]. \quad (\text{C.8})$$

Thus, as claimed in the main text, we have the lower bounds

$$P_T(N, c) \geq \max \{ P \in \{2, \dots, 2^N\} : NP \mathbb{P}[T_{DN}(\boldsymbol{\xi}^1)_1 \neq \xi_2^1] \leq c \} \quad (\text{C.9})$$

and

$$P_S(N, c) \geq \max \{ P \in \{2, \dots, 2^N\} : NP \mathbb{P}[T_{DN}(\boldsymbol{\xi}^1)_1 \neq \xi_2^1] \leq c \}. \quad (\text{C.10})$$

As introduced in the main text, for perfect recall, we want to take the threshold c to be zero, or at least to tend to zero as N and P tend to infinity. The capacities estimated through this argument are lower bounds on the true capacities, as they are obtained from lower bounds on the true recall probability. However, we expect for these bounds to in fact be tight in the thermodynamic limit [33, 34].

By the definition of the DenseNet update rule with interaction function f given in Equation (2), we have

$$T_{DN}(\boldsymbol{\xi}^1)_1 = \text{sgn} \left[\sum_{\mu=1}^P \xi_1^{\mu+1} f \left(\frac{1}{N-1} \sum_{j=2}^N \xi_j^\mu \xi_j^1 \right) \right] \quad (\text{C.11})$$

and therefore the single-bitflip probability is

$$\mathbb{P}[T_{DN}(\boldsymbol{\xi}^1)_1 \neq \xi_1^2] = \mathbb{P} \left[\text{sgn} \left[\sum_{\mu=1}^P \xi_1^{\mu+1} f \left(\frac{1}{N-1} \sum_{j=2}^N \xi_j^\mu \xi_j^1 \right) \right] \neq \xi_1^2 \right] \quad (\text{C.12})$$

$$= \mathbb{P} \left[\xi_1^2 \sum_{\mu=1}^P \xi_1^{\mu+1} f \left(\frac{1}{N-1} \sum_{j=2}^N \xi_j^\mu \xi_j^1 \right) < 0 \right] \quad (\text{C.13})$$

$$= \mathbb{P} \left[f(1) + \xi_1^2 \sum_{\mu=2}^P \xi_1^{\mu+1} f \left(\frac{1}{N-1} \sum_{j=2}^N \xi_j^\mu \xi_j^1 \right) < 0 \right] \quad (\text{C.14})$$

For both the polynomial ($f(x) = x^d$) and exponential ($f(x) = e^{(N-1)(x-1)}$) interaction functions, $f(1) = 1$, and so

$$\mathbb{P}[T_{DN}(\boldsymbol{\xi}^1)_1 \neq \xi_1^2] = \mathbb{P} \left[\sum_{\mu=2}^P \xi_1^2 \xi_1^{\mu+1} f \left(\frac{1}{N-1} \sum_{j=2}^N \xi_j^\mu \xi_j^1 \right) < -1 \right]. \quad (\text{C.15})$$

We refer to the random variable

$$C = \sum_{\mu=2}^P \xi_1^2 \xi_1^{\mu+1} f \left(\frac{1}{N-1} \sum_{j=2}^N \xi_j^\mu \xi_j^1 \right) \quad (\text{C.16})$$

on the left-hand-side of this inequality as the *crossstalk*, because it represents the effect of interference between the first pattern and all other patterns [25, 36].

We now observe that, as we have excluded self-interactions (i.e., the sum over neurons inside the interaction function does not include $j = 1$), we can use the periodic boundary conditions to shift indices as $\xi_1^\mu \leftarrow \xi_1^{\mu+1}$ for all μ , yielding

$$C \stackrel{d}{=} \sum_{\mu=2}^P \xi_1^1 \xi_1^\mu f \left(\frac{1}{N-1} \sum_{j=2}^N \xi_j^\mu \xi_j^1 \right) \quad (\text{C.17})$$

Thus, the single-bitflip probability for this DenseNet is identical to that for the corresponding MHN with symmetric interactions. Then, we can use the fact that $\xi_j^\mu \xi_j^1 \stackrel{d}{=} \xi_j^\mu$ for all $\mu = 2, \dots, P$ to obtain

$$C \stackrel{d}{=} \sum_{\mu=2}^P \xi_1^\mu f \left(\frac{1}{N-1} \sum_{j=2}^N \xi_j^\mu \right). \quad (\text{C.18})$$

Now, define the $P - 1$ random variables

$$\chi^\mu = \xi_1^\mu f \left(\frac{1}{N-1} \sum_{j=2}^N \xi_j^\mu \right) \quad (\text{C.19})$$

for $\mu = 2, \dots, P$, such that the crosstalk is their sum,

$$C = \sum_{\mu=2}^P \chi^\mu. \quad (\text{C.20})$$

As the patterns ξ_j^μ are i.i.d., χ^μ are i.i.d. random variables of mean

$$\mathbb{E}[\chi^\mu] = \mathbb{E}[\xi_1^\mu] \mathbb{E} \left[f \left(\frac{1}{N-1} \sum_{j=2}^N \xi_j^\mu \right) \right] = 0 \quad (\text{C.21})$$

and variance

$$\text{var}(\chi^\mu) = \mathbb{E} \left[f \left(\frac{1}{N-1} \sum_{j=2}^N \xi_j^\mu \right)^2 \right], \quad (\text{C.22})$$

which is bounded from above for any sensible interaction function. We observe also that the distribution of each χ^μ is symmetric because of the symmetry of the distribution of ξ_1^μ . We will therefore simply write χ for any given χ^μ .

Then, the classical central limit theorem implies that the crosstalk tends in distribution to a Gaussian of mean zero and variance $(P - 1) \text{var}(\chi)$ as $P \rightarrow \infty$, at least for any fixed N . However, we are interested in the joint limit in which $N, P \rightarrow \infty$ together. We will proceed by approximating the distribution of C as Gaussian, and will not attempt to rigorously control its behavior in the joint limit.

Approximating the distribution of the crosstalk for $N, P \gg 1$ by a Gaussian, we then have

$$\mathbb{P}[T_{DN}(\boldsymbol{\xi}^1)_1 \neq \xi_1^2] \approx H \left(\frac{1}{\sqrt{(P-1) \text{var}(\chi)}} \right) \quad (\text{C.23})$$

where $H(x) = \text{erfc}(x/\sqrt{2})/2$ is the Gaussian tail distribution function. We want to have $\mathbb{P}[T_{DN}(\boldsymbol{\xi}^1)_1 \neq \xi_1^2] \rightarrow 0$, so we must have $(P - 1) \text{var}(\chi) \rightarrow 0$. Then, we can use the asymptotic expansion [25]

$$H(\sqrt{z}) = \frac{1}{\sqrt{2\pi z}} \exp\left(-\frac{z}{2}\right) \left[1 + \mathcal{O}\left(\frac{1}{z}\right) \right] \quad \text{as } z \rightarrow \infty \quad (\text{C.24})$$

to obtain

$$\mathbb{P}[T_{DN}(\boldsymbol{\xi}^1)_1 \neq \xi_1^2] \approx \sqrt{\frac{(P-1) \text{var}(\chi)}{2\pi}} \exp\left(-\frac{1}{2(P-1) \text{var}(\chi)}\right). \quad (\text{C.25})$$

For each model, we can evaluate $\text{var}(\chi)$ and then determine the resulting predicted capacity.

As we did for the classic Hopfield network in Appendix B, we can estimate the capacity at finite c within the Gaussian approximation by inverting the Gaussian tail distribution function. Concretely, under the union bound, we can estimate the transition capacity by solving

$$c = NH \left(\frac{1}{\sqrt{(P_T - 1) \text{var}(\chi)}} \right), \quad (\text{C.26})$$

which yields

$$P_T - 1 = \frac{1}{\text{var}(\chi) [H^{-1}(c/N)]^2}, \quad (\text{C.27})$$

and the sequence capacity by solving the transcendental self-consistent equation

$$c = NP_S H \left(\frac{1}{\sqrt{(P_S - 1) \text{var}(\chi)}} \right), \quad (\text{C.28})$$

which we can re-write as

$$P_S - 1 = \frac{1}{\text{var}(\chi) [H^{-1}(c/NP_S)]^2}. \quad (\text{C.29})$$

As in the classic Hopfield case, we can simplify these complicated equations somewhat by assuming that c/N and $c/(NP_S)$ are small. Concretely, using the asymptotic

$$[H^{-1}(x)]^2 \sim -2 \log(x) \quad (\text{C.30})$$

for $x \rightarrow 0$, the transition capacity simplifies to

$$P_T - 1 \sim \frac{1}{2 \text{var}(\chi) \log(N)} \quad (\text{C.31})$$

under the assumption that $-\log(c)$ is negligible relative to $\log(N)$. For the sequence capacity, we can follow an identical argument to that used for the classic Hopfield network to simplify the self-consistent equation to

$$P_S \sim \frac{1}{2 \text{var}(\chi) \log(NP_S)} \quad (\text{C.32})$$

under the assumption that $-\log(c)$ is negligible relative to $\log(NP_S)$, which we can solve to obtain

$$P_S \sim \frac{1}{2 \text{var}(\chi) W_0[N/2 \text{var}(\chi)]}. \quad (\text{C.33})$$

Assuming that $N/\text{var}(\chi) \rightarrow \infty$ as $N \rightarrow \infty$, we can use the asymptotic $W_0(N) \sim \log(N)$ to obtain the asymptotic

$$P_S \sim \frac{1}{2 \text{var}(\chi) \log[N/\text{var}(\chi)]}. \quad (\text{C.34})$$

Our first check on the accuracy of the Gaussian approximation will be comparison of the resulting predictions for capacity with numerical experiment. As another diagnostic, we will consider the excess kurtosis $\varkappa = \kappa_4(C)/\kappa_2(C)$ for $\kappa_n(C)$ the n -th cumulant of C . If the distribution is indeed Gaussian, the excess kurtosis vanishes, while large values of the excess kurtosis indicate deviations from Gaussianity. By the additivity of cumulants, we have

$$\kappa_n(C) = (P - 1)\kappa_n(\chi). \quad (\text{C.35})$$

By symmetry, all odd cumulants of χ —and therefore all odd cumulants of C —are identically zero. As noted above, we have

$$\text{var}(\chi) = \kappa_2(\chi) = \mathbb{E} \left[f \left(\frac{1}{N-1} \sum_{j=2}^N \xi_j^\mu \right)^2 \right]. \quad (\text{C.36})$$

If C is indeed Gaussian, then all cumulants above the second should vanish. As the third cumulant vanishes by symmetry, the leading possible correction to Gaussianity is the fourth cumulant, which as χ has zero mean is given by

$$\kappa_4(\chi) = \mathbb{E}[(\chi)^4] - 3\mathbb{E}[(\chi)^2]^2 \quad (\text{C.37})$$

$$= \mathbb{E} \left[f \left(\frac{1}{N-1} \sum_{j=2}^N \xi_j^\mu \right)^4 \right] - 3\mathbb{E} \left[f \left(\frac{1}{N-1} \sum_{j=2}^N \xi_j^\mu \right)^2 \right]^2. \quad (\text{C.38})$$

Rather than considering the fourth cumulant directly, we will consider the excess kurtosis

$$\varkappa = \frac{\kappa_4(C)}{\kappa_2(C)^2} = \frac{1}{P-1} \frac{\kappa_4(\chi)}{\kappa_2(\chi)^2}, \quad (\text{C.39})$$

which is a more useful metric because it is normalized.

1. Polynomial DenseNet Capacity

We first consider the Polynomial DenseNet, with interaction function $f(x) = x^d$ for $d \in \mathbb{N}_{>0}$. To compute the capacity, our goal is then to evaluate

$$\text{var}(\chi) = \mathbb{E} \left[\left(\frac{1}{N-1} \sum_{j=2}^N \xi_j^1 \right)^{2d} \right] \quad (\text{C.40})$$

at large N . From the central limit theorem, we expect

$$\mathbb{E} \left[\left(\frac{1}{N-1} \sum_{j=2}^N \xi_j^1 \right)^{2d} \right] \sim \frac{(2d-1)!!}{(N-1)^d}. \quad (\text{C.41})$$

We can make this quantitatively precise through the following straightforward argument. Let

$$\Xi = \frac{1}{\sqrt{N-1}} \sum_{j=2}^N \xi_j^2. \quad (\text{C.42})$$

We then have immediately that the moment generating function of Ξ is

$$M(t) = \mathbb{E}[e^{t\Xi}] = \cosh \left(\frac{t}{\sqrt{N-1}} \right)^{N-1}, \quad (\text{C.43})$$

hence the cumulant generating function is

$$K(t) = \log M(t) = (N-1) \log \cosh \left(\frac{t}{\sqrt{N-1}} \right). \quad (\text{C.44})$$

The function $x \mapsto \log \cosh(x)$ is an even function of x , and is analytic near the origin, with the first few orders of its MacLaurin series being

$$\log \cosh(x) = \frac{x^2}{2} - \frac{x^4}{12} + \mathcal{O}(x^6). \quad (\text{C.45})$$

Then, the odd cumulants of Ξ vanish—as we expect from symmetry—while the even cumulants obey

$$\kappa_{2k} = \frac{C_{2k}}{(N-1)^{k-1}} \quad (\text{C.46})$$

for combinatorial factors C_{2k} that do not scale with N . We have, in particular, $C_2 = 1$ and $C_4 = -2$. By the moments-cumulants formula, we have

$$\mathbb{E}[\Xi^{2k}] = B_{2k}(0, \kappa_2, 0, \kappa_4, \dots, \kappa_{2k}) \quad (\text{C.47})$$

for B_{2k} the $2k$ -th complete exponential Bell polynomial. From this, it follows that

$$\mathbb{E}[\Xi^{2k}] = (2k - 1)!! + \mathcal{O}(N^{-1}), \quad (\text{C.48})$$

as all cumulants other than $\kappa_2 = 1$ are $\mathcal{O}(N^{-1})$. Therefore, neglecting subleading terms, we have

$$\text{var}(\chi) = \mathbb{E} \left[\left(\frac{1}{N-1} \sum_{j=2}^N \xi_j^1 \right)^{2d} \right] = \frac{(2d-1)!!}{N^d} \left[1 + \mathcal{O} \left(\frac{1}{N} \right) \right]. \quad (\text{C.49})$$

Following the general arguments above, we then approximate

$$\mathbb{P}[T_{DN}(\boldsymbol{\xi}^1)_1 \neq \xi_1^2] \sim \sqrt{\frac{P(2d-1)!!}{2\pi N^d}} \exp \left(-\frac{N^d}{2P(2d-1)!!} \right). \quad (\text{C.50})$$

To determine the single-transition capacity following the argument in Section II A, we must determine how large we can take $P = P(N)$ such that $N\mathbb{P}[T_{DN}(\boldsymbol{\xi}^1)_1 \neq \xi_1^2] \rightarrow 0$. Following the requirement that $P \text{var}(\chi) \rightarrow 0$, we make the *Ansatz*

$$P \sim \frac{N^d}{\alpha(2d-1)!! \log N} \quad (\text{C.51})$$

for some α . We then have

$$N\mathbb{P}[T_{DN}(\boldsymbol{\xi}^1)_1 \neq \xi_1^2] \sim \sqrt{\frac{1}{2\pi\alpha \log N}} N^{1-\alpha/2}. \quad (\text{C.52})$$

This tends to zero if $\alpha \geq 2$, meaning that the predicted capacity in this case is

$$P_T \sim \frac{N^d}{2(2d-1)!! \log N}. \quad (\text{C.53})$$

We now want to determine the sequence capacity, which requires the stronger condition $NPP[T_{DN}(\boldsymbol{\xi}^1)_1 \neq \xi_1^2] \rightarrow 0$. Again making the *Ansatz*

$$P \sim \frac{N^d}{\alpha(2d-1)!! \log N} \quad (\text{C.54})$$

for some α , we then have

$$NPP[T_{DN}(\boldsymbol{\xi}^1)_1 \neq \xi_1^2] \sim \frac{1}{\sqrt{2\pi}(2d-1)!! (\alpha \log N)^{3/2}} N^{d+1-\alpha/2}, \quad (\text{C.55})$$

which tends to zero if $\alpha \geq 2d+2$. Then, the predicted sequence capacity is

$$P_S \sim \frac{N^d}{2(d+1)(2d-1)!! \log N}. \quad (\text{C.56})$$

If we consider the alternative asymptotic formulas obtained above from the finite- c argument, we have

$$P_T \sim \frac{1}{2 \text{var}(\chi) \log(N)} \sim \frac{N^d}{2(2d-1)!! \log(N)} \quad (\text{C.57})$$

and

$$P_S \sim \frac{1}{2 \text{var}(\chi) \log[N/\text{var}(\chi)]} \sim \frac{N^d}{2(2d-1)!! \log[N^{d+1}/(2d-1)!!]} \sim \frac{N^d}{2(d+1)(2d-1)!! \log(N)}, \quad (\text{C.58})$$

which agree with these results.

Using the Gaussian approximation for moments of χ given above, we can easily work out that

$$\kappa_4(\chi) = \mathbb{E}[(\chi)^4] - 3\mathbb{E}[(\chi)^2] \quad (\text{C.59})$$

$$= \mathbb{E} \left[f \left(\frac{1}{N-1} \sum_{j=2}^N \xi_j^\mu \right)^4 \right] - 3\mathbb{E} \left[f \left(\frac{1}{N-1} \sum_{j=2}^N \xi_j^\mu \right)^2 \right]^2 \quad (\text{C.60})$$

$$= \frac{1}{N^{2d}} \{ (4d-1)!! - 3[(2d-1)!!]^2 \} \left[1 + \mathcal{O} \left(\frac{1}{N} \right) \right]. \quad (\text{C.61})$$

Then, the excess kurtosis of the Polynomial DenseNet's crosstalk is

$$\varkappa = \frac{1}{P-1} \left[\frac{(4d-1)!!}{[(2d-1)!!]^2} - 3 \right] \left[1 + \mathcal{O} \left(\frac{1}{N} \right) \right]. \quad (\text{C.62})$$

Thus, for the Polynomial DenseNet, we expect the excess kurtosis to be small for any fixed d so long as P and N are both fairly large, without any particular requirement on their relationship. In particular, under the Gaussian approximation we predicted above that the transition and sequence capacities should both scale as

$$P \sim \frac{N^d}{\alpha_d \log N}, \quad (\text{C.63})$$

where α_d depends on d but not on N . This gives an excess kurtosis of

$$\varkappa = \frac{\alpha_d \log N}{N^d} \left[\frac{(4d-1)!!}{[(2d-1)!!]^2} - 3 \right] \left[1 + \mathcal{O} \left(\frac{1}{N} \right) \right] \quad (\text{C.64})$$

which for any fixed d rapidly tends to zero with increasing N . This suggests that the Gaussian approximation should be reasonably accurate even at modest N , but of course does not constitute a proof of its accuracy because we have not considered higher cumulants. However, this matches the results of numerical simulations shown in Figure 2.

2. Exponential DenseNet capacity

We now turn our attention to the Exponential DenseNet, with separation function $f(x) = e^{(N-1)(x-1)}$. In this case, we have

$$\text{var}(\chi) = \exp[-2(N-1)] \mathbb{E} \left[\exp \left(2 \sum_{j=2}^N \xi_j^2 \right) \right] \quad (\text{C.65})$$

$$= \exp[-2(N-1)] \prod_{j=2}^N \mathbb{E} [\exp(2\xi_j^2)] \quad (\text{C.66})$$

$$= \exp[-2(N-1)] \cosh(2)^{N-1} \quad (\text{C.67})$$

$$= \frac{1}{\beta^{N-1}}, \quad (\text{C.68})$$

where we have defined the constant

$$\beta = \frac{\exp(2)}{\cosh(2)} \simeq 1.96403. \quad (\text{C.69})$$

Then, we have the Gaussian approximation

$$\mathbb{P}[T_{DN}(\boldsymbol{\xi}^1)_1 \neq \xi_1^2] \sim \sqrt{\frac{P}{2\pi\beta^{N-1}}} \exp \left(-\frac{\beta^{N-1}}{2P} \right). \quad (\text{C.70})$$

As in the polynomial case, we first determine the single-transition capacity by demanding that $N\mathbb{P}[T_{DN}(\boldsymbol{\xi}^1)_1 \neq \xi_1^2] \rightarrow 0$. We plug in the *Ansatz*

$$P \sim \frac{\beta^{N-1}}{\alpha \log N} \quad (\text{C.71})$$

for some α , which yields

$$N\mathbb{P}[T_{DN}(\boldsymbol{\xi}^1)_1 \neq \xi_1^2] \sim \sqrt{\frac{1}{2\pi\alpha \log N}} N^{1-\alpha/2}. \quad (\text{C.72})$$

This tends to zero if $\alpha \geq 2$, which gives a predicted capacity of

$$P_T \sim \frac{\beta^{N-1}}{2 \log N}. \quad (\text{C.73})$$

Considering the sequence capacity, which again requires that $N\mathbb{P}[T_{DN}(\boldsymbol{\xi}^1)_1 \neq \xi_1^2] \rightarrow 0$, we plug in the *Ansatz*

$$P \sim \frac{\beta^{N-1}}{\alpha N}, \quad (\text{C.74})$$

which yields

$$N\mathbb{P}[T_{DN}(\boldsymbol{\xi}^1)_1 \neq \xi_1^2] \sim \frac{1}{\alpha\beta} \sqrt{\frac{1}{2\pi\alpha N}} \exp\left[\left(\log \beta - \frac{\alpha}{2}\right) N\right]. \quad (\text{C.75})$$

This tends to zero for $\alpha \geq 2 \log \beta$, meaning that the predicted capacity is in this case

$$P_S \sim \frac{\beta^{N-1}}{2 \log(\beta) N}. \quad (\text{C.76})$$

Therefore, while the ratio of the predicted single-transition to sequence capacities is finite for the Polynomial DenseNet—it is simply $P_S/P_T \sim d + 1$ —for the Exponential DenseNet it tends to zero as $P_S/P_T \sim \log N / [\log(\beta) N]$.

Using the asymptotic formulas obtained above from the finite- c argument, we have

$$P_T \sim \frac{1}{2 \text{var}(\chi) \log(N)} = \frac{\beta^{N-1}}{2 \log(N)} \quad (\text{C.77})$$

and

$$P_S \sim \frac{1}{2 \text{var}(\chi) \log[N / \text{var}(\chi)]} = \frac{\beta^{N-1}}{2 \log[N\beta^{N-1}]} \sim \frac{\beta^{N-1}}{2 \log(\beta) N}, \quad (\text{C.78})$$

which agree with these results.

Now considering the fourth cumulant, we can easily compute

$$\kappa_4(\chi) = \left(\frac{\cosh(4)}{\exp(4)}\right)^{N-1} - 3 \left(\frac{\cosh(2)^2}{\exp(4)}\right)^{N-1}, \quad (\text{C.79})$$

which yields an excess kurtosis of

$$\varkappa = \frac{1}{P-1} \left[\left(\frac{\cosh(4)}{\cosh(2)^2}\right)^{N-1} - 3 \right]. \quad (\text{C.80})$$

For this to be small, P must be exponentially large in N , which contrasts with the situation for the Polynomial DenseNet, in which the excess kurtosis is small for any reasonably large P . If we consider taking

$$P \sim \frac{\beta^{N-1}}{\alpha \log N}, \quad (\text{C.81})$$

for a constant α , as the Gaussian theory predicts for the Exponential DenseNet transition capacity, we have

$$\varkappa \sim \frac{\alpha \log N}{\beta^{N-1}} \left[\left(\frac{\cosh(4)}{\cosh(2)^2} \right)^{N-1} - 3 \right] \quad (\text{C.82})$$

$$\sim \alpha \log N \left(\frac{\cosh(4)}{\exp(2) \cosh(2)} \right)^{N-1} \quad (\text{C.83})$$

$$\simeq \alpha \log(N) (0.9823)^{N-1}. \quad (\text{C.84})$$

This tends to zero as N increases, but only very slowly. In particular, $\log(N)(0.9823)^{N-1}$ increases with N up to around $N \simeq 19$, where it attains a maximum value around 2, before decreasing towards zero. The situation is even worse for the sequence capacity, for which the Gaussian theory predicts

$$P \sim \frac{\beta^{N-1}}{\alpha N}, \quad (\text{C.85})$$

yielding

$$\varkappa \sim \frac{\alpha N}{\beta^{N-1}} \left[\left(\frac{\cosh(4)}{\cosh(2)^2} \right)^{N-1} - 3 \right] \quad (\text{C.86})$$

$$\sim \alpha N \left(\frac{\cosh(4)}{\exp(2) \cosh(2)} \right)^{N-1} \quad (\text{C.87})$$

$$\simeq \alpha N (0.9823)^{N-1}. \quad (\text{C.88})$$

$N(0.9823)^{N-1}$ increases with N up to around $N \simeq 56$, where it attains a value of approximately 21.

Taken together, these results suggest that we might expect substantial finite-size corrections to the Gaussian theory's prediction for the capacity. In particular, as the excess kurtosis of the crosstalk is positive, the tails of the crosstalk distribution should be heavier-than-Gaussian, suggesting that the Gaussian theory should overestimate the true capacity. This holds provided that the lower bound on the memorization probability resulting from the union bound is reasonably tight.

Appendix D: Generalized pseudoinverse rule capacity

Here, we show that the generalized pseudoinverse rule can perfectly recall any sequence of linearly-independent patterns. We recall from (11) that the GPI update rule is

$$T_{GPI}(\mathbf{S})_i = \text{sgn} \left[\sum_{\mu=1}^P \xi_i^{\mu+1} f \left(\sum_{\nu=1}^P (O^+)^{\mu\nu} m^\nu(\mathbf{S}) \right) \right] \quad (\text{D.1})$$

for

$$O^{\mu\nu} = \frac{1}{N} \sum_{j=1}^N \xi_j^\mu \xi_j^\nu \quad (\text{D.2})$$

the Gram matrix of the patterns. If the patterns are linearly independent, then \mathbf{O} is full rank, and the pseudoinverse reduces to the ordinary inverse: $\mathbf{O}^+ = \mathbf{O}^{-1}$. Under this assumption, we have

$$T_{GPI}(\boldsymbol{\xi}^\mu)_i = \text{sgn} \left[\sum_{\nu=1}^P \xi_i^{\nu+1} f(\delta^{\mu\nu}) \right] \quad (\text{D.3})$$

$$= \text{sgn} \left[f(1) \xi_i^{\mu+1} + f(0) \sum_{\nu \neq \mu} \xi_i^{\nu+1} \right], \quad (\text{D.4})$$

for all μ and i , hence for separation functions satisfying $f(1) > 0$ and $|f(0)| < f(1)/(P-1)$ we are guaranteed to have $T_{GPI}(\boldsymbol{\xi}^\mu)_i = \xi_i^{\mu+1}$ as desired. For $f(x) = x^d$, this condition is always satisfied as $f(0) = 0$ and $f(1) = 1$. For $f(x) = e^{(N-1)(x-1)}$, we have $f(0) = e^{-(N-1)}$ and $f(1) = 1$; the condition $P-1 < e^{N-1}$ must therefore be satisfied. However, as $P \leq N$ is required for linear independence, this condition is satisfied so long as $N > 3$.

Appendix E: MixedNet Capacity

In this Appendix, we compute the capacity of the mixed network, which from the update rule defined in (13) has

$$T_{MN}(\xi^1)_1 = \text{sgn} \left\{ \sum_{\mu=1}^P \left[\xi_1^\mu f_S \left(\frac{1}{N-1} \sum_{j=2}^N \xi_j^\mu \xi_j^1 \right) + \lambda \xi_1^{\mu+1} f_A \left(\frac{1}{N-1} \sum_{j=2}^N \xi_j^\mu \xi_j^1 \right) \right] \right\}. \quad (\text{E.1})$$

Then, assuming that $f_S(1) = f_A(1) = 1$ as is true for the interaction functions considered here, we have

$$\mathbb{P}[T_{MN}(\xi^1)_1 \neq \xi_1^2] \quad (\text{E.2})$$

$$= \mathbb{P} \left\{ \xi_1^2 \left[\sum_{\mu=1}^P \xi_1^\mu f_S \left(\frac{1}{N-1} \sum_{j=2}^N \xi_j^\mu \xi_j^1 \right) + \lambda \sum_{\mu=1}^P \xi_1^{\mu+1} f_A \left(\frac{1}{N-1} \sum_{j=2}^N \xi_j^\mu \xi_j^1 \right) \right] < 0 \right\} \quad (\text{E.3})$$

$$= \mathbb{P}\{C < -\lambda\}, \quad (\text{E.4})$$

where we have defined the crosstalk

$$C = \xi_1^2 \xi_1^1 + \sum_{\mu=2}^P \xi_1^2 \xi_1^\mu f_S \left(\frac{1}{N-1} \sum_{j=2}^N \xi_j^\mu \xi_j^1 \right) + \lambda \sum_{\mu=2}^P \xi_1^2 \xi_1^{\mu+1} f_A \left(\frac{1}{N-1} \sum_{j=2}^N \xi_j^\mu \xi_j^1 \right). \quad (\text{E.5})$$

For $j = 2, \dots, N$ and $\mu = 2, \dots, P$, we have the equality in distribution $\xi_j^\mu \xi_j^1 \stackrel{d}{=} \xi_j^\mu$, hence

$$C \stackrel{d}{=} \xi_1^2 \xi_1^1 + \sum_{\mu=2}^P \xi_1^2 \xi_1^\mu f_S(\Xi^\mu) + \lambda \sum_{\mu=2}^P \xi_1^2 \xi_1^{\mu+1} f_A(\Xi^\mu). \quad (\text{E.6})$$

where to lighten our notation we define

$$\Xi^\mu = \frac{1}{N-1} \sum_{j=2}^N \xi_j^\mu. \quad (\text{E.7})$$

However, unlike in the DenseNet, we cannot similarly simplify the terms outside the separation functions. Recalling that we have assumed periodic boundary conditions, we have

$$C = \xi_1^2 \xi_1^1 + \lambda \xi_1^2 \xi_1^1 f_A(\Xi^P) + f_S(\Xi^2) + \sum_{\mu=3}^P \xi_1^2 \xi_1^\mu f_S(\Xi^\mu) + \lambda \sum_{\mu=2}^{P-1} \xi_1^2 \xi_1^{\mu+1} f_A(\Xi^\mu) \quad (\text{E.8})$$

$$\stackrel{d}{=} \xi_1^1 + C_1 + C_2 + C_3 + C_4, \quad (\text{E.9})$$

where we have defined

$$C_1 = f_S(\Xi^2) + \lambda \xi_1^3 f_A(\Xi^2), \quad (\text{E.10})$$

$$C_2 = \xi_1^P f_S(\Xi^P) + \lambda \xi_1^1 f_A(\Xi^P), \quad (\text{E.11})$$

$$C_3 = \sum_{\mu=3}^{P-1} \xi_1^\mu f_S(\Xi^\mu), \quad \text{and} \quad (\text{E.12})$$

$$C_4 = \lambda \sum_{\mu=3}^{P-1} \xi_1^{\mu+1} f_A(\Xi^\mu). \quad (\text{E.13})$$

Importantly, in this case the influence of ξ_1^1 on the crosstalk is $\mathcal{O}(1)$, and the distribution is not well-approximated by a single Gaussian. Instead, as shown in Figure E.1, it is bimodal. We will therefore approximate it by a mixture of two Gaussians, one for each value of ξ_1^1 . This approximation can be justified by noting that the boundary terms in C_1 and C_2 should be negligible at large N and P , while C_3 and C_4 should give a Gaussian contribution at sufficiently large P . We now observe that, for any f_S and f_A , the conditional means of each term are

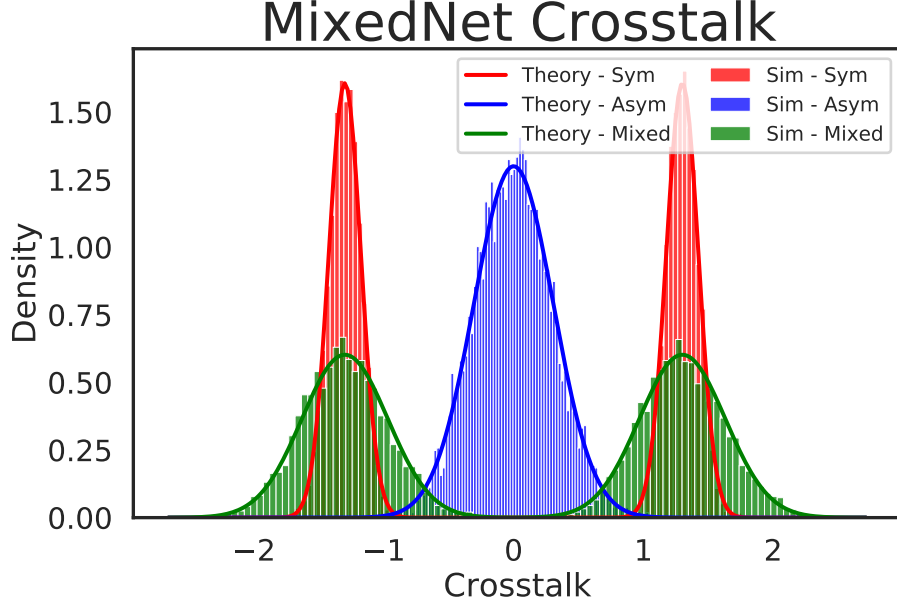


FIG. E.1. Crosstalk of Polynomial MixedNet where $N = 100$, $\lambda = 2.5$, $d_S = d_A = 3$ and $P = 1000$ patterns are stored. Histograms are generated for patterns drawn from 5000 randomly sequences and theoretical curves are plotted. Green represents the full crosstalk for the MixedNet. Blue and red represent the asymmetric and symmetric terms of the crosstalk, respectively. Observe that the bimodality in the full model comes from bimodality in the symmetric term.

$$\mathbb{E}[C_1 | \xi_1^1] = \mathbb{E}[f_S(\Xi)] \quad (\text{E.14})$$

$$\mathbb{E}[C_2 | \xi_1^1] = \lambda \xi_1^1 \mathbb{E}[f_A(\Xi)] \quad (\text{E.15})$$

$$\mathbb{E}[C_3 | \xi_1^1] = 0 \quad (\text{E.16})$$

$$\mathbb{E}[C_4 | \xi_1^1] = 0, \quad (\text{E.17})$$

where we note that all Ξ 's are identically distributed, so we can simply write Ξ for any one of them. Then, the conditional mean of the crosstalk is

$$\mathbb{E}[C | \xi_1^1] = \xi_1^1 + \sum_{j=1}^4 \mathbb{E}[C_j | \xi_1^1] \quad (\text{E.18})$$

$$= \xi_1^1 \{1 + \lambda \mathbb{E}[f_A(\Xi)]\} + \mathbb{E}[f_S(\Xi)]. \quad (\text{E.19})$$

Considering the variance of C , the variances of the different contributions are

$$\text{var}[C_1 | \xi_1^1] = \text{var}[f_S(\Xi)] + \lambda^2 \mathbb{E}[f_A(\Xi)^2] \quad (\text{E.20})$$

$$\text{var}[C_2 | \xi_1^1] = \mathbb{E}[f_S(\Xi)^2] + \lambda^2 \text{var}[f_A(\Xi)] \quad (\text{E.21})$$

$$\text{var}[C_3 | \xi_1^1] = (P - 3) \mathbb{E}[f_S(\Xi)^2] \quad (\text{E.22})$$

$$\text{var}[C_4 | \xi_1^1] = \lambda^2 (P - 3) \mathbb{E}[f_A(\Xi)^2], \quad (\text{E.23})$$

while the covariances are

$$\text{cov}[C_1, C_2 | \xi_1^1] = 0 \quad (\text{E.24})$$

$$\text{cov}[C_1, C_3 | \xi_1^1] = \lambda \mathbb{E}[f_A(\Xi)] \mathbb{E}[f_S(\Xi)] \quad (\text{E.25})$$

$$\text{cov}[C_1, C_4 | \xi_1^1] = 0, \quad (\text{E.26})$$

$$\text{cov}[C_2, C_3 | \xi_1^1] = 0 \quad (\text{E.27})$$

$$\text{cov}[C_2, C_4 | \xi_1^1] = \lambda \mathbb{E}[f_S(\Xi)] \mathbb{E}[f_A(\Xi)], \quad (\text{E.28})$$

and

$$\text{cov}[C_3, C_4 | \xi_1^1] = \lambda \sum_{\mu, \nu=3}^{P-1} \mathbb{E}[\xi_1^\mu \Xi_1^{\nu+1}] \mathbb{E}[f_S(\Xi^\mu) f_A(\Xi^\nu)] \quad (\text{E.29})$$

$$= \lambda \sum_{\mu=3}^P \mathbb{E}[f_S(\Xi^\mu)] \mathbb{E}[f_A(\Xi^{\mu-1})] \quad (\text{E.30})$$

$$= \lambda(P-3) \mathbb{E}[f_S(\Xi)] \mathbb{E}[f_A(\Xi)]. \quad (\text{E.31})$$

Therefore, the conditional variance of the crosstalk is

$$\text{var}[C | \xi_1^1] = \sum_{j=1}^4 \text{var}[C_j | \xi_1^1] + 2 \sum_{j=1}^4 \sum_{k>j} \text{cov}[C_j, C_k | \xi_1^1] \quad (\text{E.32})$$

$$= (P-3) \{ \mathbb{E}[f_S(\Xi)^2] + 2\lambda \mathbb{E}[f_S(\Xi)] \mathbb{E}[f_A(\Xi)] + \lambda^2 \mathbb{E}[f_A(\Xi)^2] \} \\ + \text{var}[f_S(\Xi)] + \lambda^2 \mathbb{E}[f_A(\Xi)^2] + \mathbb{E}[f_S(\Xi)^2] + \lambda^2 \text{var}[f_A(\Xi)] + 4\lambda \mathbb{E}[f_A(\Xi)] \mathbb{E}[f_S(\Xi)] \quad (\text{E.33})$$

$$= (P-1) \{ \mathbb{E}[f_S(\Xi)^2] + 2\lambda \mathbb{E}[f_S(\Xi)] \mathbb{E}[f_A(\Xi)] + \lambda^2 \mathbb{E}[f_A(\Xi)^2] \} \\ - \mathbb{E}[f_S(\Xi)]^2 - \lambda^2 \mathbb{E}[f_A(\Xi)]^2. \quad (\text{E.34})$$

For large P and N , the two terms on the second line of this result will be subleading, as they do not scale with P and have identical or subleading scaling with N to the terms that do scale with P . That is, we have

$$\text{var}[C | \xi_1^1] \sim P \{ \mathbb{E}[f_S(\Xi)^2] + 2\lambda \mathbb{E}[f_S(\Xi)] \mathbb{E}[f_A(\Xi)] + \lambda^2 \mathbb{E}[f_A(\Xi)^2] \}. \quad (\text{E.35})$$

Collecting these results, we have

$$\mathbb{E}[C | \xi_1^1] = \xi_1^1 \{ 1 + \lambda \mathbb{E}[f_A(\Xi)] \} + \mathbb{E}[f_S(\Xi)] \quad (\text{E.36})$$

and

$$\text{var}[C | \xi_1^1] \sim P \{ \mathbb{E}[f_S(\Xi)^2] + 2\lambda \mathbb{E}[f_S(\Xi)] \mathbb{E}[f_A(\Xi)] + \lambda^2 \mathbb{E}[f_A(\Xi)^2] \}. \quad (\text{E.37})$$

By the law of total probability, we have

$$\mathbb{P}[T_{MN}(\boldsymbol{\xi}^1)_1 \neq \xi_1^2] = \mathbb{P}[C < -\lambda] \quad (\text{E.38})$$

$$= \frac{1}{2} \mathbb{P}[C < -\lambda | \xi_1^1 = -1] + \frac{1}{2} \mathbb{P}[C < -\lambda | \xi_1^1 = +1] \quad (\text{E.39})$$

$$\sim \frac{1}{2} H \left(\frac{\lambda + \mathbb{E}[C | \xi_1^1 = -1]}{\sqrt{\text{var}[C | \xi_1^1 = -1]}} \right) + \frac{1}{2} H \left(\frac{\lambda + \mathbb{E}[C | \xi_1^1 = +1]}{\sqrt{\text{var}[C | \xi_1^1 = +1]}} \right) \quad (\text{E.40})$$

under the bimodal Gaussian approximation to the crosstalk distribution. To have $\mathbb{P}[T_{MN}(\boldsymbol{\xi}^1)_1 \neq \xi_1^2]$, both of these conditional probabilities must tend to zero. By basic concentration arguments, we expect to have

$$\mathbb{E}[C | \xi_1^1] \sim \xi_1^1 \quad (\text{E.41})$$

up to corrections that are small in an absolute sense. Moreover, we have

$$\mathbb{E}[C | \xi_1^1 = +1] - \mathbb{E}[C | \xi_1^1 = -1] = 2 \{ 1 + \lambda \mathbb{E}[f_A(\Xi)] \} \quad (\text{E.42})$$

which for the separation functions considered here is strictly positive. As we keep λ constant with N and P , we must have

$$\mathbb{E}[C | \xi_1^1 = -1] > -\lambda \quad (\text{E.43})$$

and $\text{var}[C | \xi_1^1 = -1] \rightarrow 0$ in order to have $\mathbb{P}[T_{MN}(\boldsymbol{\xi}^1)_1 \neq \xi_1^2] \rightarrow 0$. But, given the formula above, $\text{var}[C | \xi_1^1 = -1] = \text{var}[C | \xi_1^1 = +1]$, so this implies that the $\xi_1^1 = +1$ contribution to the probability will be exponentially suppressed. hen,

we can apply an identical argument to that which we used for the DenseNet in Appendix C to obtain the asymptotic behavior of $\mathbb{P}[C < -\lambda | \xi_1^1 = -1]$, yielding

$$\mathbb{P}[T_{MN}(\xi^1)_1 \neq \xi_1^2] \sim \frac{1}{2} H \left(\frac{\lambda + \mathbb{E}[C | \xi_1^1 = -1]}{\sqrt{\text{var}[C | \xi_1^1 = -1]}} \right) \quad (\text{E.44})$$

$$\sim \frac{1}{2\sqrt{2\pi}} \frac{\sqrt{\text{var}[C | \xi_1^1 = -1]}}{\lambda + \mathbb{E}[C | \xi_1^1 = -1]} \exp \left(-\frac{1}{2} \frac{(\lambda + \mathbb{E}[C | \xi_1^1 = -1])^2}{\text{var}[C | \xi_1^1 = -1]} \right). \quad (\text{E.45})$$

For this to work, we must clearly have $\lambda > 1$.

We could in principle compute the excess kurtosis of the crosstalk for the MixedNet as we did for the DenseNet, but we will not do so here as the computation would be tedious and would not yield substantial new insight beyond that for the DenseNet.

1. Polynomial MixedNet

We first consider the polynomial mixed network, with $f_S(x) = x^{d_S}$ and $f_A(x) = x^{d_A}$ for two possibly differing degrees $d_S, d_A \in \mathbb{N}_{>0}$. We can apply the same reasoning as in Appendix C1 to obtain the required moments at large N , which yields the first moments

$$\mathbb{E}[f_S(\Xi)] = \mathbb{E}[\Xi^{d_S}] = \begin{cases} 0 & d_S \text{ odd,} \\ \frac{(d_S - 1)!!}{N^{d_S/2}} \left[1 + \mathcal{O}\left(\frac{1}{N}\right) \right] & d_S \text{ even} \end{cases} \quad (\text{E.46})$$

and

$$\mathbb{E}[f_A(\Xi)] = \mathbb{E}[\Xi^{d_A}] = \begin{cases} 0 & d_A \text{ odd,} \\ \frac{(d_A - 1)!!}{N^{d_A/2}} \left[1 + \mathcal{O}\left(\frac{1}{N}\right) \right] & d_A \text{ even,} \end{cases} \quad (\text{E.47})$$

and the second moments

$$\mathbb{E}[f_S(\Xi)^2] = \mathbb{E}[\Xi^{2d_S}] = \frac{(2d_S - 1)!!}{N^{d_S}} \left[1 + \mathcal{O}\left(\frac{1}{N}\right) \right] \quad (\text{E.48})$$

and

$$\mathbb{E}[f_A(\Xi)^2] = \mathbb{E}[\Xi^{2d_A}] = \frac{(2d_A - 1)!!}{N^{d_A}} \left[1 + \mathcal{O}\left(\frac{1}{N}\right) \right]. \quad (\text{E.49})$$

Then, the conditional mean of the crosstalk is given by

$$\mathbb{E}[C | \xi_1^1] \sim \xi_1^1 \quad (\text{E.50})$$

up to corrections which vanish in an absolute, not a relative, sense, while the conditional variance is asymptotic to

$$\text{var}[C | \xi_1^1] \sim P \left\{ \frac{(2d_S - 1)!!}{N^{d_S}} + 2\lambda \frac{(d_S - 1)!! (d_A - 1)!!}{N^{(d_S + d_A)/2}} \mathbf{1}\{d_S, d_A \text{ even}\} + \lambda^2 \frac{(2d_A - 1)!!}{N^{d_A}} \right\}. \quad (\text{E.51})$$

We must now determine the storage capacity. We recall that, in all case, we want P to tend to infinity slowly enough that $\text{var}[C | \xi_1^1]$ tends to zero. Then, we can see that what matters is which of the terms inside the curly brackets in the expression for the conditional variance above tends to zero with N the slowest. This is of course determined by $\min\{d_S, d_A\}$, but the constant factor multiplying the leading term will depend on which is smaller, or if they are equal. First, consider the case in which $d_S = d_A = d$. Then, we have

$$\text{var}[C | \xi_1^1] \sim \frac{P}{N^d} \left\{ (2d - 1)!! + 2\lambda (d - 1)!! (d - 1)!! \mathbf{1}\{d \text{ even}\} + \lambda^2 (2d - 1)!! \right\}. \quad (\text{E.52})$$

Now, consider the case in which $d_S < d_A$. Then, $(d_S + d_A)/2 > d_S$, hence the N^{-d_S} term dominates and we have

$$\text{var}[C | \xi_1^1] \sim \frac{P}{N^{d_S}} (2d_S - 1)!!. \quad (\text{E.53})$$

Similarly, if $d_A > d_S$, the N^{-d_A} term dominates, and we have

$$\text{var}[C | \xi_1^1] \sim \frac{P}{N^{d_A}} \lambda^2 (2d_A - 1)!! \quad (\text{E.54})$$

We can summarize these results as

$$\text{var}[C | \xi_1^1] \sim \gamma_{d_S, d_A} \frac{P}{N^{\min\{d_S, d_A\}}}, \quad (\text{E.55})$$

where

$$\gamma_{d_S, d_A} = \begin{cases} (2d_S - 1)!! & \text{if } d_S < d_A, \\ (\lambda^2 + 1)(2d_S - 1)!! + 2\lambda[(d_S - 1)!!]^2 \mathbf{1}\{d_S \text{ even}\} & \text{if } d_S = d_A, \\ \lambda^2(2d_A - 1)!! & \text{if } d_S > d_A. \end{cases} \quad (\text{E.56})$$

Using the general arguments presented above, we then have

$$\mathbb{P}[T_{MN}(\boldsymbol{\xi}^1)_1 \neq \xi_1^2] \sim \frac{1}{2\sqrt{2\pi}} \sqrt{\frac{\gamma_{d_S, d_A} P}{(\lambda - 1)^2 N^{\min\{d_S, d_A\}}}} \exp\left(-\frac{(\lambda - 1)^2 N^{\min\{d_S, d_A\}}}{2 \gamma_{d_S, d_A} P}\right). \quad (\text{E.57})$$

for any $\lambda > 1$. We must first determine the single-transition capacity, which requires that $N\mathbb{P}[T_{MN}(\boldsymbol{\xi}^1)_1 \neq \xi_1^2] \rightarrow 0$. Recalling that our argument requires us to take $P \rightarrow \infty$ slowly enough that $\text{var}[C | \xi_1^1] \rightarrow 0$, we make the *Ansatz* that

$$P \sim \frac{(\lambda - 1)^2 N^{\min\{d_S, d_A\}}}{\alpha \gamma_{d_S, d_A} \log N} \quad (\text{E.58})$$

for some α . This yields

$$N\mathbb{P}[T_{MN}(\boldsymbol{\xi}^1)_1 \neq \xi_1^2] \sim \frac{1}{2\sqrt{2\pi\alpha} \log N} N^{1-\alpha/2}, \quad (\text{E.59})$$

which tends to zero if $\alpha \geq 2$, yielding a predicted capacity of

$$P_T \sim \frac{(\lambda - 1)^2 N^{\min\{d_S, d_A\}}}{2\gamma_{d_S, d_A} \log N}. \quad (\text{E.60})$$

We now consider the sequence capacity, which requires that $NP\mathbb{P}[T_{MN}(\boldsymbol{\xi}^1)_1 \neq \xi_1^2] \rightarrow 0$. Then, making the same *Ansatz* for P as above, we have

$$NP\mathbb{P}[T_{MN}(\boldsymbol{\xi}^1)_1 \neq \xi_1^2] \sim \frac{1}{2\sqrt{2\pi}} \frac{(\lambda - 1)^2}{\gamma_{d_S, d_A}} \frac{1}{(\alpha \log N)^{3/2}} N^{\min\{d_S, d_A\} + 1 - \alpha/2}, \quad (\text{E.61})$$

which tends to zero provided that $\alpha \geq 2(\min\{d_S, d_A\} + 1)$, yielding a predicted capacity of

$$P_S \sim \frac{(\lambda - 1)^2}{2(\min\{d_S, d_A\} + 1)\gamma_{d_S, d_A}} \frac{N^{\min\{d_S, d_A\}}}{\log N}. \quad (\text{E.62})$$

2. Exponential MixedNet

We now consider the Exponential MixedNet, with $f_S(x) = f_A(x) = e^{(N-1)(x-1)}$. With this, we have the first moments

$$\mathbb{E}[f_S(\Xi)] = \mathbb{E}[f_A(\Xi)] = \exp[-(N-1)] \mathbb{E}\left[\exp\left(\sum_{j=2}^N \xi_j\right)\right] \quad (\text{E.63})$$

$$= \exp[-(N-1)] \prod_{j=2}^N \mathbb{E}[\exp(\xi_j)] \quad (\text{E.64})$$

$$= \left(\frac{\cosh(1)}{\exp(1)}\right)^{N-1} \quad (\text{E.65})$$

and the second moments

$$\mathbb{E}[f_S(\Xi)^2] = \mathbb{E}[f_A(\Xi)^2] = \left(\frac{\cosh(2)}{\exp(2)} \right)^{N-1} = \frac{1}{\beta^{N-1}}, \quad (\text{E.66})$$

where as in Appendix C 2 we let

$$\beta = \frac{\exp(2)}{\cosh(2)} \simeq 1.96403. \quad (\text{E.67})$$

Noting that

$$\frac{\exp(1)}{\cosh(1)} \simeq 1.76159, \quad (\text{E.68})$$

the conditional mean of the crosstalk is then

$$\mathbb{E}[C | \xi_1^1] = \xi_1^1 \{1 + \lambda \mathbb{E}[f_A(\Xi)]\} + \mathbb{E}[f_S(\Xi)] \quad (\text{E.69})$$

$$= \xi_1^1 \left\{ 1 + \lambda \left(\frac{\cosh(1)}{\exp(1)} \right)^{N-1} \right\} + \left(\frac{\cosh(1)}{\exp(1)} \right)^{N-1} \quad (\text{E.70})$$

$$\sim \xi_1^1, \quad (\text{E.71})$$

where the corrections are exponentially small in an absolute sense. The leading part of the conditional variance of the crosstalk is

$$\text{var}[C | \xi_1^1] \sim P \{ \mathbb{E}[f_S(\Xi)^2] + 2\lambda \mathbb{E}[f_S(\Xi)] \mathbb{E}[f_A(\Xi)] + \lambda^2 \mathbb{E}[f_A(\Xi)^2] \} \quad (\text{E.72})$$

$$\sim \frac{P}{\beta^{N-1}} \left\{ 1 + 2\lambda \left(\frac{\cosh(1)^2}{\cosh(2)} \right)^{N-1} + \lambda^2 \right\} \quad (\text{E.73})$$

$$\sim \frac{P}{\beta^{N-1}} (1 + \lambda^2), \quad (\text{E.74})$$

where we note that

$$\frac{\cosh(1)^2}{\cosh(2)} \simeq 0.632901 \quad (\text{E.75})$$

hence the other contribution is exponentially suppressed in a relative sense.

We thus have

$$\mathbb{E}[C | \xi_1^1] \sim \xi_1^1 \quad (\text{E.76})$$

$$\text{var}[C | \xi_1^1] \sim \frac{P}{\beta^{N-1}} (1 + \lambda^2), \quad (\text{E.77})$$

hence from the general argument above we have

$$\mathbb{P}[T_{MN}(\xi^1)_1 \neq \xi_1^2] \sim \frac{1}{2\sqrt{2\pi}} \frac{\sqrt{(1+\lambda^2)}}{\lambda-1} \sqrt{\frac{P}{\beta^{N-1}}} \exp\left(-\frac{1}{2} \frac{(\lambda-1)^2 \beta^{N-1}}{1+\lambda^2} \frac{1}{P}\right) \quad (\text{E.78})$$

for $\lambda > 1$. We now want to determine the capacity, starting with the single-transition capacity, for which we must have $N\mathbb{P}[T_{MN}(\xi^1)_1 \neq \xi_1^2] \rightarrow 0$. Recalling that we want to have $\text{var}[C | \xi_1^1] \rightarrow 0$, we make the *Ansatz*

$$P \sim \frac{1}{\alpha} \frac{(\lambda-1)^2 \beta^{N-1}}{\lambda^2 + 1 \log N} \quad (\text{E.79})$$

for some α , which yields

$$N\mathbb{P}[T_{MN}(\xi^1)_1 \neq \xi_1^2] \sim \frac{1}{2\sqrt{2\pi\alpha \log N}} N^{1-\alpha/2}. \quad (\text{E.80})$$

This tends to zero if $\alpha \geq 2$, hence we conclude that the Gaussian theory predicts

$$P_T \sim \frac{1}{2} \frac{(\lambda - 1)^2}{\lambda^2 + 1} \frac{\beta^{N-1}}{\log N}. \quad (\text{E.81})$$

We now want to determine the sequence capacity, which requires that $NPP[T_{MN}(\xi^1)_1 \neq \xi_1^2] \rightarrow 0$. Following our analysis of the Exponential DenseNet in Appendix C2, we make the *Ansatz* that

$$P \sim \frac{1}{\alpha} \frac{(\lambda - 1)^2}{\lambda^2 + 1} \frac{\beta^{N-1}}{N}, \quad (\text{E.82})$$

which yields

$$NPP[T_{MN}(\xi^1)_1 \neq \xi_1^2] \sim \frac{1}{2\sqrt{2\pi\alpha N}} \frac{1}{\alpha\beta} \frac{(\lambda - 1)^2}{\lambda^2 + 1} \exp\left[\left(\log\beta - \frac{\alpha}{2}\right)N\right]. \quad (\text{E.83})$$

This tends to zero if $\alpha \geq 2 \log\beta$, giving a predicted sequence capacity of

$$P_S = \frac{1}{2 \log\beta} \frac{(\lambda - 1)^2}{\lambda^2 + 1} \frac{\beta^{N-1}}{N}. \quad (\text{E.84})$$

Thus, for both definitions of capacity, the Gaussian theory’s prediction of the capacity of the Exponential MixedNet is

$$\frac{(\lambda - 1)^2}{\lambda^2 + 1} \quad (\text{E.85})$$

times the capacity of the Exponential DenseNet analyzed in Appendix C2. This factor tends to zero from above as $\lambda \downarrow 1$, and gradually increases to 1 as $\lambda \rightarrow \infty$. Note that even without explicitly computing the excess kurtosis, we expect the intuition from the Exponential DenseNet to carry over to this setting. Indeed, the numerical simulations in Figure 9 show that the transition capacity is well captured by the Gaussian theory while the sequence capacity shows significant deviation for small MixedNets.

Appendix F: Numerical implementation

Source code will be made available on GitHub upon acceptance. Experiments were run on the Harvard University FAS RC Cannon HPC cluster (<https://www.rc.fas.harvard.edu/>), using Nvidia A100 80GB GPUs. This limited the maximum number of patterns we could store in memory simultaneously to approximately 10^6 patterns, restricting our experimental evaluation of the Exponential DenseNet to approximately $N = 25$ neurons.

1. Transition capacity

Numerical simulations for transition capacity were conducted as follows: For a given model of size N , start by initializing 100 sequences of Rademacher distributed patterns of length P_0 , where $P_0 = 2P^*$ is well above the model’s predicted capacity P^* . This initialization for P_0 was found through trial and error, where the method detects if you start below capacity. The model’s update rule is applied in parallel across all patterns and across all sequences. If errors are made for any pattern in any sequence, 100 new random sequences are generated with smaller length $P_1 = 0.99P_0$. This is repeated, with the new sequence length being $P_{t+1} = 0.99P_t$, until 100 sequences are generated for which no error is made in any transition. This entire process is repeated 20 times starting from P_0 in order to obtain error bars.

2. Sequence capacity

Numerical simulations for sequence capacity were conducted in a similar fashion. For a given model of size N , start by initializing 100 sequences of Rademacher distributed patterns of length P_0 , where P_0 is well above the model’s capacity. Starting from the first pattern of each sequence, the model’s update rule is applied serially for each sequence. As soon as an error is obtained within any sequence, 100 new random sequences are generated with smaller length $P_1 = 0.99P_0$. This is repeated, with the new sequence length being $P_{t+1} = 0.99P_t$, until 100 sequences are generated for which no error is made. This entire process is repeated 20 times starting from P_0 in order to obtain error bars.

3. MNIST

For the MNIST experiments in Section IID, MNIST images were pre-processed to have binarized pixel values [67]. They were then sorted into subsequences of unique images ranging from 0 to 9, and 1000 unique subsequences were concatenated to construct the entire sequence. Then, different models were run from initialization and their output for different time steps was displayed in Figure 5.

4. Generalized pseudoinverse rule

For numerical simulations of the generalized pseudoinverse rule in IIE, the transition capacity of the Polynomial DenseNet was simulated in a similar method as described above. However, the Exponential DenseNet suffered from numerical instability when calculating the pseudoinverse of the overlap matrix, resulting in floating point error. Therefore, we showed results only for the Polynomial DenseNet.